JOURNAL OF GEOPHYSICAL RESEARCH, VOL. 106, NO. B8, PAGES 16,177–16,204, AUGUST 10, 2001

Geochronologic and thermobarometric constraints on the evolution of the Main Central Thrust, central Nepal Himalaya

E. J. Catlos,[1] T. Mark Harrison,[1] Matthew J. Kohn,[2] Marty Grove,[3] F. J. Ryerson,[4] Craig E. Manning,[3] and B. N. Upreti[5]

Abstract. The Main Central Thrust (MCT) juxtaposes the high-grade Greater Himalayan Crystallines over the lower-grade Lesser Himalaya Formation; an apparent inverted metamorphic sequence characterizes the shear zone that underlies the thrust. Garnet-bearing assemblages sampled along the Marysandi River and Darondi Khola in the Annapurna region of central Nepal show striking differences in garnet zoning of Mn, Ca, Mg, and Fe above and below the MCT. Thermobarometry of MCT footwall rocks yields apparent inverted temperature and pressure gradients of ~18°C km^{-1} and ~0.06 km MPa^{-1}, respectively. Pressure-temperature (P-T) paths calculated for upper Lesser Himalaya samples that preserve prograde compositions show evidence of decompression during heating, whereas garnets from the structurally lower sequences grew during an increase in both pressure and temperature. In situ (i.e., analyzed in thin section) ion microprobe ages of monazites from rocks immediately beneath the Greater Himalayan Crystallines yield ages from 18 to 22 Ma, whereas late Miocene and Pliocene monazite ages characterize rocks within the apparent inverted metamorphic sequence. A Lesser Himalayan sample collected near the garnet isograd along the Marysandi River transect contains 3.3±0.1 Ma monazite ages (P ≈ 0.72 GPa, T ≈ 535°C). This remarkably young age suggests that this portion of the MCT shear zone accommodated a minimum of ~30 km of slip over the last 3 Ma (i.e., a slip rate of >10 mm yr^{-1}) and thus could account for nearly half of the convergence across the Himalaya in this period. The distribution of ages and P-T histories reported here are consistent with a thermokinematic model in which the inverted metamorphic sequences underlying the MCT formed by the transposition of right-way-up metamorphic sequences during late Miocene-Pliocene shearing.

1. Introduction

The relatively narrow Himalayan arc extends ~2400 km from Nanga Parbat (8138 m) in the west to Namche Barwa (7756 m) in the east [e.g., *Le Fort*, 1996]. This mountain belt forms a sharp transition between the average ~5-km-high, arid Tibetan Plateau and the warmer, wetter Indian lowlands and is composed of roughly parallel, crustal-scale fault systems separating similar lithologies along strike.

The Main Central Thrust (MCT) is the dominant crustal thickening structure in the Himalaya, accommodating from 140 km to >500 km of displacement [*Schelling and Arita*, 1991; *Srivastava and Mitra*, 1994]. The fault is underlain by a 2- to 12-km-thick sequence of deformed rocks known as the MCT shear zone. At most locations, footwall rocks display an increase in metamorphic intensity toward structurally higher levels, and metamorphic facies are generally continuous across the fault [e.g., *Pêcher*, 1989]. The inverted isograds are sometimes interpreted as a relict inverted geotherm, and their origin is the subject of numerous models [e.g., *Le Fort*, 1975; *England et al.*, 1992; *Hubbard*, 1996; *Huerta et al.*, 1996; *Harrison et al.*, 1998]. The nature of the anomalous gradient has important implications for the roles that thermal sources (e.g., shear heating, magma bodies, radiogenic elements) and heat transfer mechanisms (e.g., advection, accretion-erosion processes) play in crustal deformation.

This paper presents thermobarometric and geochronologic data from rocks collected adjacent to the MCT along the Marysandi River and Darondi Khola, central Nepal. Metamorphic pressure-temperature (P-T) histories were obtained from thermobarometric analyses of garnet-bearing assemblages. Monazite and, in some cases, garnet growth ages were determined from in situ ion microprobe analyses. Muscovite $^{40}Ar/^{39}Ar$ analyses were undertaken to assess the retrograde cooling history. The combined results indicate that the apparent Himalayan inverted metamorphism is actually due to the accretion of successive footwall slivers to the hanging wall during late Miocene-Pliocene activity within the MCT shear zone [*Harrison et al.*, 1998].

[1]Department of Earth and Space Sciences and Institute of Geophysics and Planetary Physics, University of California, Los Angeles.
[2]Department of Geological Sciences, University of South Carolina, Columbia, South Carolina.
[3]Department of Earth and Space Sciences, University of California, Los Angeles.
[4]Institute for Geophysics and Planetary Physics, Lawrence Livermore National Laboratory, Livermore, California.
[5]Department of Geology, Tri-Chandra Campus, Tribhuvan University, Kathmandu, Nepal.

Paper number 2000JB900375.
0148-0227/01/2000JB900375$09.00

2. Geologic Background

2.1. Orogen-Scale Description of the Himalaya

The MCT is one of five large-scale fault systems that formed as a result of the Indo-Asia collision [*Gansser*, 1981; *Pêcher*, 1989; *Schelling*, 1992; *Le Fort*, 1996] (Plate 1). The Indus Tsangpo Suture Zone juxtaposes Indian shelf sediments (Tethys metasediments) against Asian metasedimentary and igneous rocks [*Yin et al.*, 1994; *Quidelleur et al.*, 1997]. The north dipping South Tibetan Detachment System separates low-grade Cambrian to mid-Eocene Tethys Formation rocks in its hanging wall from a 5- to 20-km-thick late Proterozoic unit of footwall gneisses called the Greater Himalayan Crystallines [*Burg et al.*, 1984; *Valdiya*, 1988; *Burchfiel et al.*, 1992]. At their base the Greater Himalayan Crystallines are thrust over Middle Proterozoic phyllites, metaquartzites, and mylonitic augen gneisses of the Lesser Himalaya Formation along the MCT [*Arita*, 1983; *Brunel and Kienast*, 1986; *Pêcher*, 1989]. Farther south, the Main Boundary Thrust (MBT) separates the Lesser Himalaya from Neogene molasse, the Siwalik Formation [*Seeber et al.*, 1981; *Valdiya*, 1992; *Meigs et al.*, 1995]. South of the MBT, the Main Frontal Thrust (MFT) typically defines the boundary between the Siwalik and northern Indo-Gangetic Plains [*Le Fort*, 1996]. The MFT cuts Siwalik strata in places and is often manifested as anticline growth [*Yeats et al.*, 1992; *Powers et al.*, 1998]. These structures appear to sole into a decollement termed the Main Himalayan Thrust (MHT) [*Zhao et al.*, 1993; *Nelson et al.*, 1996]. Two roughly parallel chains of granites intrude the Tethys Formation and upper structural levels of the Greater Himalayan Crystallines [*Le Fort*, 1975; *Harrison et al.*, 1997].

The Indian craton moves north-northeast at a rate of 44-61 mm yr^{-1} relative to Eurasia/Siberia [*Minster and Jordan*, 1978; *Armijo et al.*, 1986; *DeMets et al.*, 1990], although recent global positioning studies suggest the present rate may be significant slower at 37-42 mm yr^{-1} [*Chen et al.*, 2000; *Shen et al.*, 2000]. The active faults within the Himalaya include the MBT with a seismic slip rate of ~4 mm yr^{-1} [*Ye et al.*, 1981; *Valdiya*, 1992] and the MFT, which accommodates N-S shortening from 9 to 21 mm yr^{-1} [*Lyon-Caen and Molnar*, 1983; *Baker et al.*, 1988; *Yeats et al.*, 1992; *Powers et al.*, 1998; *Lavé and Avouac*, 2000]. A clearly identifiable, ~50-km-wide zone of predominately moderate earthquakes is located within the Lesser Himalaya, south of the MCT [*Seeber et al.*, 1981; *Khattri and Tyagi*, 1983; *Valdiya*, 1992; *Kayal*, 1996]. Seismic activity in this region may be linked to the underthrusting of the Lesser Himalaya beneath the Greater Himalayan Crystallines [*Seeber et al.*, 1981; *Valdiya*, 1994] or to part of the detachment that separates the underthrusting Indian Plate from the Lesser Himalayan crustal block [*Ni and Barazangi*, 1984].

2.2. Rocks and Structures Associated With the MCT in Central Nepal

Our investigation focuses on central Nepal (Plate 2), where most of the geologic elements characteristic of the Himalaya are exposed, including leucogranites, inverted metamorphism, and the MCT [e.g., *Colchen et al.*, 1980; *Pêcher and Le Fort*, 1986; *England et al.*, 1992; *Coleman*, 1996a; *Hodges et al.*, 1996].

2.2.1. Greater Himalayan Crystallines. In central Nepal, the Greater Himalayan Crystallines are divided into three formations [*Pêcher and Le Fort*, 1986]. Formation I is kyanite- and sillimanite-bearing metapelites, gneisses, and metagraywackes with abundant quartzite, formation II is largely comprised of calc-silicate gneisses and marbles, and formation III is composed of augen orthogneisses. U-Pb and Sm-Nd studies of detrital zircons show that the sedimentary provenance of the Greater Himalayan Crystallines is ~1 Ga younger than that of the Lesser Himalaya [*Parrish and Hodges*, 1996]. Two metamorphic episodes were proposed for the evolution of the Greater Himalayan Crystallines in central Nepal [see *Pêcher and Le Fort*, 1986]. The first stage (Eocene-Oligocene) of Barrovian-type metamorphism, termed the Eohimalayan event, corresponds to burial of the nappe beneath the southern edge of Tibet [*Le Fort*, 1996]. During this stage the base reached 650-700°C and ~0.8 GPa. During the second stage (Miocene), termed the Neohimalayan event, the base experienced 550-600°C, while the top of the section was at lower pressures and/or temperatures. The Neohimalayan is associated with MCT slip and the development of anatectic melts exposed near the Greater Himalayan Crystallines-Tethys Formation contact [*Pêcher*, 1989].

2.2.2. South Tibetan Detachment System. The presence of the South Tibetan Detachment System in the Marysandi basin is debated. Along the Marysandi River transect, peak temperatures continuously decrease across the Greater Himalayan Crystallines-Tethys Formation boundary [*Schneider and Masch*, 1993] and field observations do not reveal a distinct structural discontinuity [e.g., *Fuchs et al.*, 1988]. It has been suggested that Formation III is the core of a recumbent anticline between similar carbonate lithologies of formation II and the lower structural levels of the Tethys Formation [*Bordet et al.*, 1975; *Fuchs et al.*, 1988, 1999]. This is in contrast to the views of several workers who place a detachment fault between the open folding of the Tethys and the homoclinal structure of the Greater Himalayan Crystallines [*Brown and Nazarchuk*, 1993; *Schneider and Mash*, 1993; *Coleman*, 1996a; *Le Fort and Guillot*, 1998]. The Manaslu Intrusive Complex records extensional structures [*Le Fort*, 1975; *Guillot et al.*, 1993], but whether these are associated with significant slip along the South Tibetan Detachment System remains unknown.

2.2.3. Lesser Himalaya and the MCT. In central Nepal (Plate 2), metamorphic grade increases from low (chlorite + biotite ± zeolite) to medium (biotite + garnet + kyanite ± staurolite) over a north-south distance of ~20 km toward the MCT, with the highest-grade Lesser Himalaya rocks found within the MCT shear zone [*Pêcher*, 1989].

Precise placement of the MCT fault is problematic because of the lack of a break in metamorphic grade between Greater Himalayan Crystallines and Lesser Himalaya. *Pêcher* [1989] adopted three criteria to discern its location: (1) the boundary between hanging wall gneisses and upper carbonate-rich formations of the Lesser Himalaya, (2) where Lesser Himalaya shear fabric (L-S) is replaced by the planar fabric of the Greater Himalayan Crystallines, and (3) where the rotational deformation that increases progressively through the Lesser Himalaya reaches a maximum. In central Nepal, *Arita* [1983] places two thrusts (MCT I and MCT II) on each side of the MCT shear zone (see Plates 2-5). The MCT II

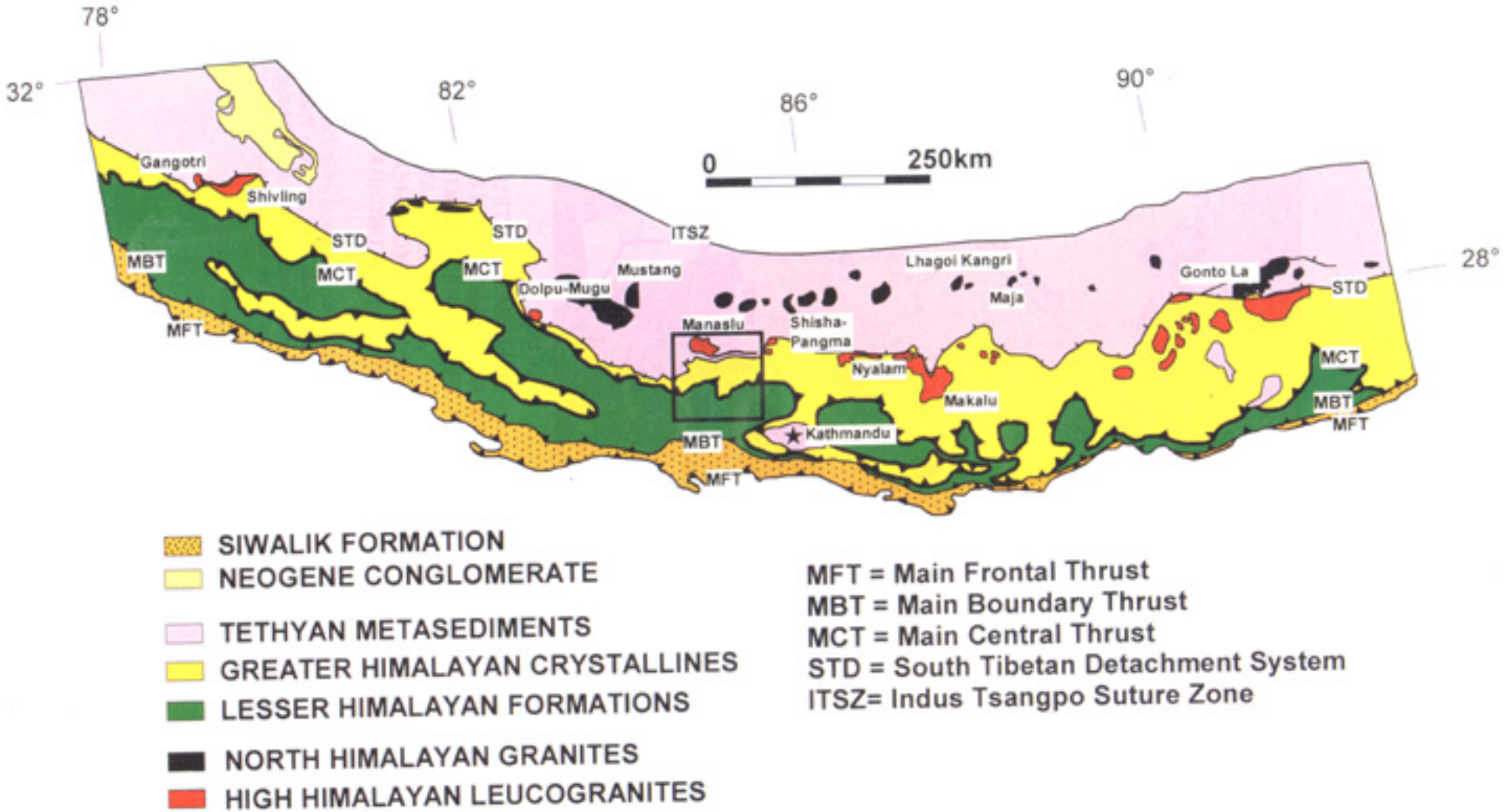

Plate 1. Geologic map of the Himalayan range in Nepal (after *LeFort* [1996]). The box outlines the boundaries of the Annapurna-Manaslu-Ganesh region of central Nepal (Plate 2). The names of some of the High Himalayan and North Himalayan granite bodies are included for reference.

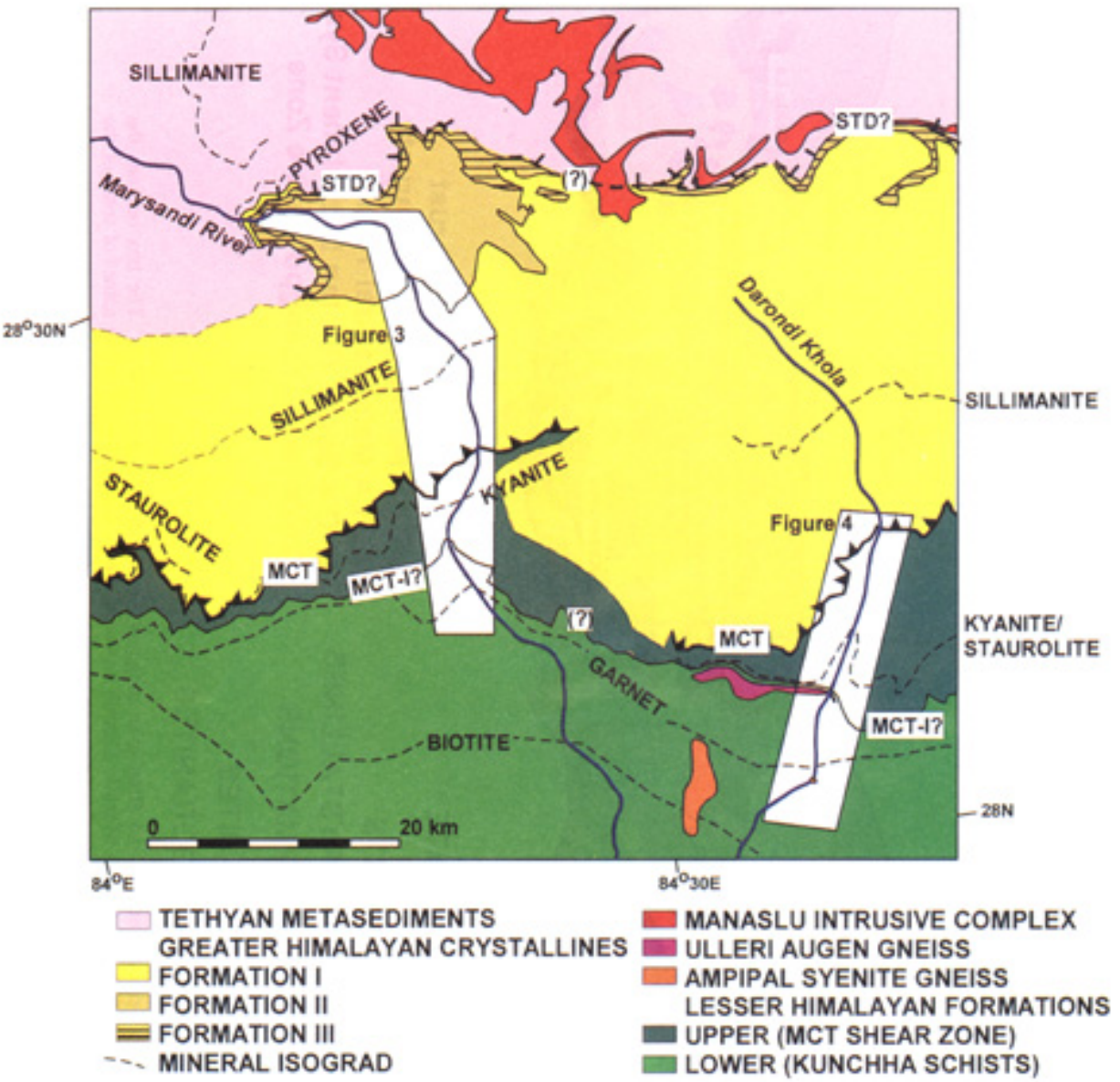

Plate 2. Geologic map of the Annapurna-Manaslu-Ganesh region of central Nepal after *Colchen et al.* [1980]. The areas outlined by the boxes are transects along the Marysandi River (left; see Plate 3) and Darondi Khola (right; see Plate 4) from which samples were collected. Isograds are dashed and labeled. The pyroxene isograd refers specifically to the metacarbonate lithologies. The question mark indicates the presence of these structures are debated.

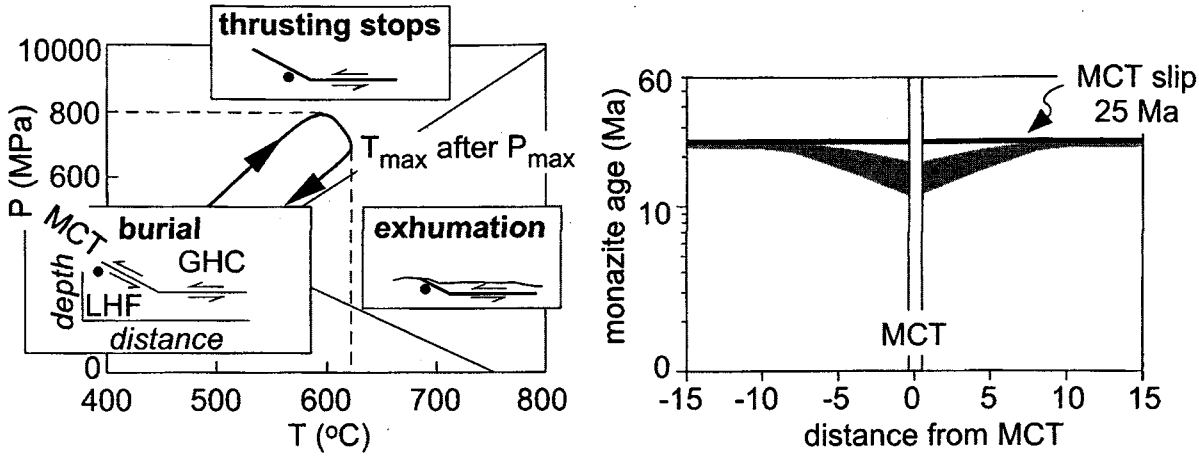

Figure 1. (left) Particle paths and a P-T path predicted for a Lesser Himalaya Formation (LHF) rock collected immediately beneath the MCT if the fault experienced a single episode of slip. In the left inset, the rock, seen as a solid circle, is buried beneath the Greater Himalayan Crystallines (GHC). In the top inset, thrusting stops and heat is supplied across the MCT ramp as indicated by the thicker line. In the right inset, the rock is exhumed by erosion. A schematic P-T path followed by this sample indicates that maximum temperature (T_{max}) is experienced after maximum pressure (P_{max}). (right) Distribution of Th-Pb monazite ages versus distance from the MCT. The upper bound of the grey distribution is for a larger grain, whereas the lower bound is for a smaller grain. Crystallization is assumed to take place only at ~25 Ma.

corresponds to the feature described by *Pêcher* [1989], whereas the MCT I separates a mylonitic augen gneiss from other Lesser Himalaya metasedimentary rocks. The existence of the MCT I is debated (see *Upreti* [1999] for a review).

3. Models Proposed for Origin of Inverted Metamorphism

Models proposed to describe the evolution of the Himalaya generally agree that the orogeny began subsequent to the late Cretaceous-early Eocene closure along the Indus Tsangpo Suture Zone [e.g., *Le Fort*, 1996; *Rowley*, 1996]. Most assume that the zone of plate convergence shifted progressively toward the foreland during mountain building. An intracontinental thrust, the MCT, formed south of the suture during the Miocene [e.g., *Hodges et al.*, 1996]. South of the MCT, the late Miocene movement occurred along the MBT [e.g., *Meigs et al.*, 1995], and presently, the MFT is active [e.g., *Yeats et al.*, 1992]. At each stage, slip was primarily accommodated by the structure closest to the Indian foreland [e.g., *Seeber and Gornitz*, 1983].

On this foundation, two broad classes of models arose seeking to explain the evolution of Himalayan inverted metamorphism. The first set proposed a significant inverted geotherm developed during MCT slip [e.g., *Le Fort*, 1975; *England and Molnar*, 1993]. The second suggested recrystallization of the footwall units occurred prior to their juxtaposition with the hanging wall [e.g., *Searle and Rex*, 1989; *Hubbard*, 1996]. Some models attempted to ascribe the origin of leucogranite magmas found in structurally higher levels of the Greater Himalayan Crystallines to slip along the MCT [*Le Fort*, 1975; *England et al.*, 1992] or South Tibetan Detachment System [*Harris et al.*, 1993; *Harris and Massey*, 1994].

P-T paths estimated from garnet-bearing assemblages are useful for evaluating the tectonic and thermal evolution of metamorphic terranes [e.g., *Spear and Selverstone*, 1983; *Spear et al.*, 1984]. Models that support the development of a significant inverted geotherm during MCT slip (e.g., the one-slip hypothesis, Figure 1) require a significantly different P-T path than those that assume recrystallization of the footwall units occurred prior to their juxtaposition with the hanging wall. For example, in the one-slip hypothesis, a footwall rock follows a P-T path in which it experiences maximum temperature after maximum pressure owing to burial and prolonged exposure to hot hanging wall rocks. A model that suggests multiple episodes of activity within the MCT shear zone (e.g., the multislip model, Figure 2) produces a "hairpin" P-T path via the burial and quick exhumation of footwall rocks. In this scenario the maximum pressure the sample experiences correlates with maximum temperature.

Footwall rocks within the multislip model should record episodes of burial and exhumation, whereas single-slip samples would experience one stage of fault movement. Younger ages within a footwall rock could be produced with the single-slip scenario only if enough thermal energy is transferred to heat the mineral grains containing radiogenic isotopes sufficiently for diffusive loss or recrystallization to occur. Establishing the metamorphic evolution recorded by rocks within the inverted metamorphic sequence can help to assess which models are most relevant to the Himalayan range.

4. Previous Work

4.1. Previous Geochronology

Previous geochronologic analyses of samples collected from the Greater Himalayan Crystallines and MCT shear zone in the central Himalaya suggest the structure was active during the Miocene [e.g., *Hodges et al.*, 1996; *Coleman*, 1998]. The last MCT-related deformation event has been suggested to occur during this time [e.g., *Schelling and Arita*,

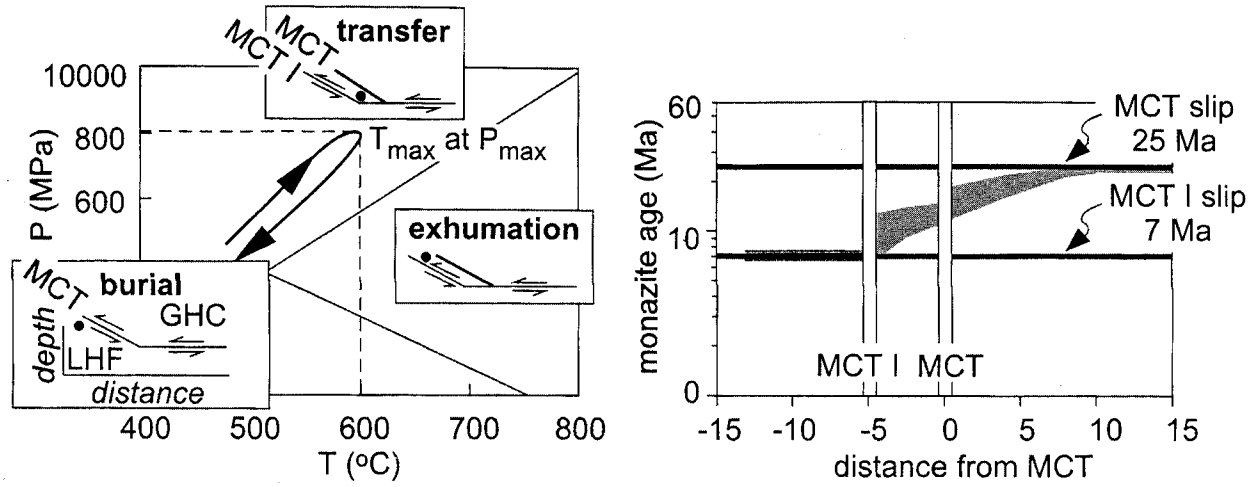

Figure 2. (left) Particle paths and a P-T path predicted for a Lesser Himalaya Formation (LHF) rock collected immediately beneath the MCT if the footwall experienced two episodes faulting. In the left inset, the rock, seen as a solid circle, is buried beneath the Greater Himalayan Crystallines (GHC). In the top inset, thrusting is transferred to another fault, the MCT I, but the MCT ramp continues to supply heat as indicated by a thicker line. In the right inset, the rock is exhumed by slip along the MCT I. A schematic P-T path followed by this sample indicates that maximum temperature (T_{max}) is experienced at maximum pressure (P_{max}). (right) Distribution of Th-Pb monazite ages versus distance from the MCT. The upper bound of the shaded distribution is for a larger grain, whereas the lower bound is for a smaller grain. Crystallization is assumed to take place at 25 Ma north of the MCT, at 15 Ma between the MCT and MCT I, and at 6 Ma south of the MCT I.

1991; *England et al.*, 1992]. Monazite grains from the MCT hanging wall contain a significant inherited Oligocene component, which appears to record the Eohimalayan event [*Hodges et al.*, 1996; *Edwards and Harrison*, 1997; *Coleman*, 1998; *Coleman and Hodges*, 1998]. The shear zone is characterized by Pliocene $^{40}Ar/^{39}Ar$ mica ages [*Copeland et al.*, 1991; *Macfarlane*, 1993; *Edwards*, 1995]. The youngest mica ages include those from the Lesser Himalaya along the Marysandi transect (2.9±0.1 Ma [*Edwards*, 1995]). *Copeland et al.* [1991] attributes the ages to thermal resetting from hot fluids, whereas *Macfarlane* [1993] suggests that they reflect a late stage brittle deformation event.

4.2. Previous Thermobarometry

Previous thermobarometric studies of the Greater Himalayan Crystallines in general (1) indicate temperatures at 600-700°C at the MCT, (2) suggest the entire section was nearly isothermal during peak conditions, and (3) indicate a decrease in pressure upsection, consistent with a lithostatic gradient [e.g., *Hodges et al.*, 1988; *Inger and Harris*, 1992; *Pognante and Benna*, 1993; *Macfarlane*, 1995; *Vannay and Hodges*, 1996]. Some studies report thermobarometric conditions inconsistent with stability of the mineral assemblage [e.g., *Brunel and Kienast*, 1986; *Hodges and Silverberg*, 1988; *Hubbard*, 1989; *Coleman*, 1996b; *Vannay and Grasemann*, 1998]. Recent reviews of Himalayan P-T data predict a majority of samples experienced retrograde net transfer reactions (ReNTRs), which involve the production and consumption of minerals used for thermobarometry [see *Kohn and Spear*, 2001]. Biotite and garnet become more Fe-rich, causing the estimated temperatures to be greater than the actual peak experienced. Thus conditions reported for the garnet-bearing rocks of the Greater Himalayan Crystallines may be erroneous by hundreds of degrees and several hundred megapascals.

Despite numerous studies of metamorphic assemblages in the hanging wall (see reviews by *Guillot* [1999] and *Macfarlane* [1999]), surprisingly little work of this kind has been undertaken on footwall samples. *Kaneko* [1995] reported footwall temperatures from rocks in central Nepal that increase toward the fault from 400-450°C to 600-650°C over a north-south distance of ~13 km. Thermobarometric analyses of Lesser Himalayan assemblages are required to quantitatively constrain metamorphic conditions, but this avenue to understanding Himalayan inverted metamorphism has been largely unexplored [see *Harrison et al.*, 1999a, Figure 3].

5. Sample Selection and Petrography from Transects in Central Nepal

Samples were collected along two cross-strike transects in central Nepal. Samples from the Marysandi River transect are referred to as MA (Plates 3 and 5a), whereas those obtained along the Darondi Khola are referred to as DH (Plates 4 and 5b). To evaluate the possible MCT I structural break [*Arita*, 1983], we divide the rocks into three domains. We chose this nomenclature in light of the thermobarometric and geochronologic data presented in this paper.

Domain 1 gneisses are from the Greater Himalayan Crystallines. Domain 2 samples are Lesser Himalayan pelites collected between the MCT and MCT I. Domain 3 rocks are Lesser Himalayan pelites and metasediments collected below the MCT I. On the basis of field observations along the Marysandi River, *Colchen et al.* [1980] mapped the MCT near the town of Bahundunda (Plate 3), but the augen gneiss

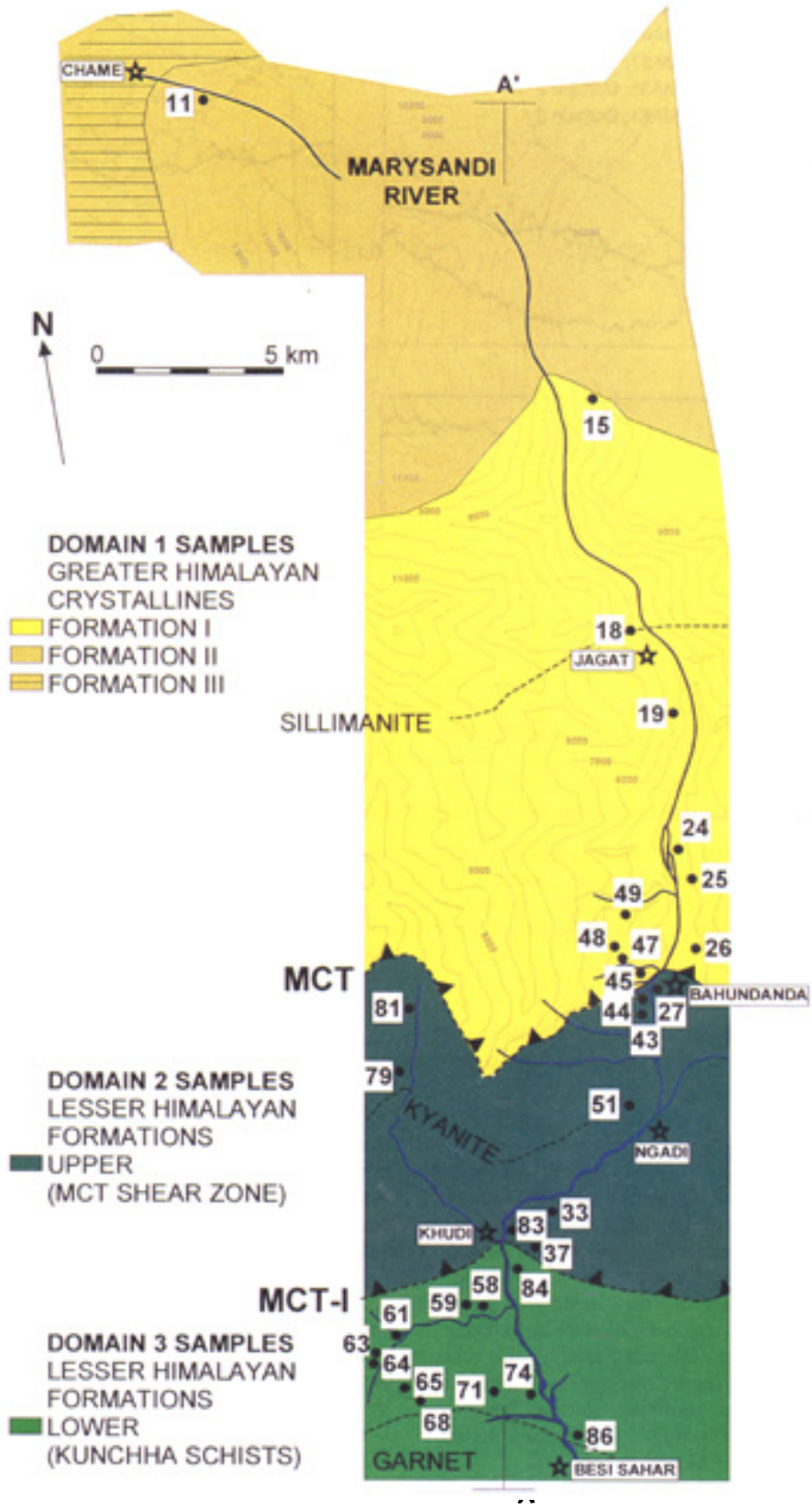

Plate 3. Sample location map from rocks collected along the Marysandi River. These samples are indicated by "MA" in the text. Town names are in boxes and designated by stars. Isograds are dashed and labeled. See Plate 5a for the cross section through A-A'.

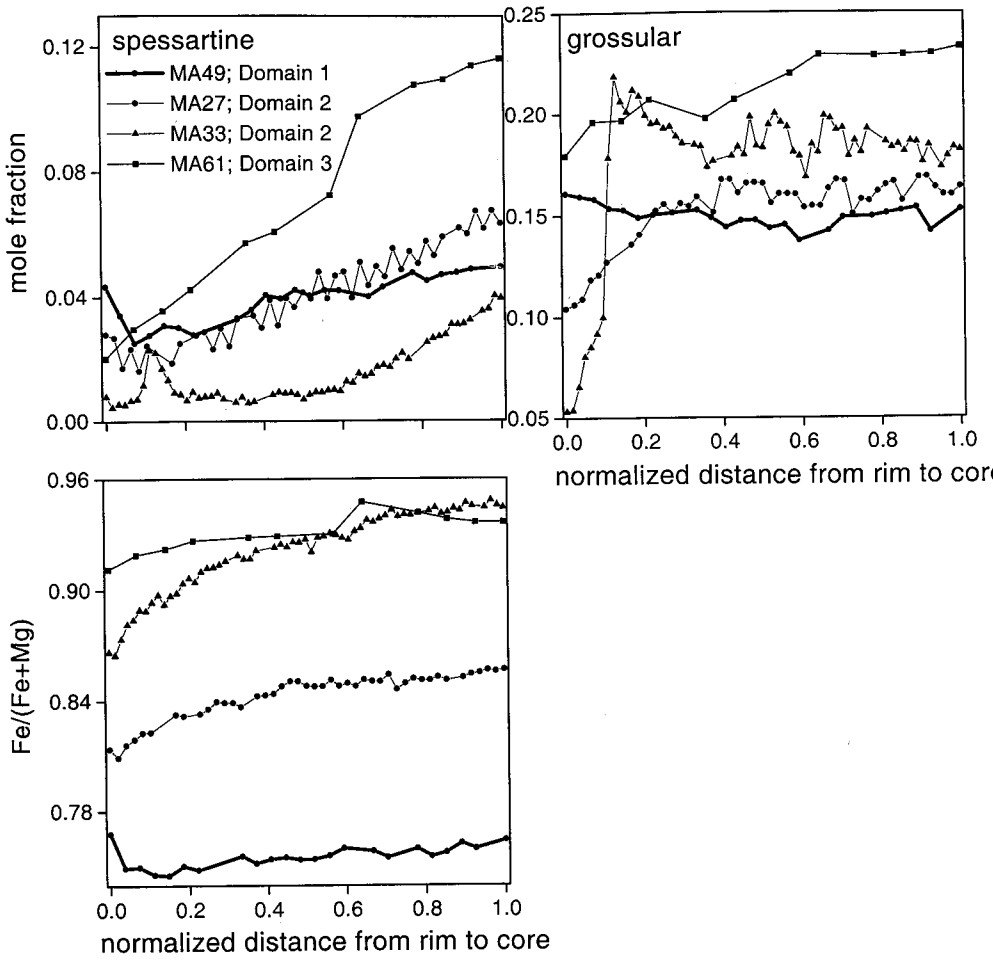

Figure 3. Mole fractions of spessartine, grossular, and Fe/(Fe+Mg) across garnets from domains 1, 2, and 3. The distance across each of these garnets is normalized (actual/ maximum distance from rim) so that 0 indicates rim, and 1.0 indicates core. X-ray element maps of these garnets are shown in Plates 6-8. For original electron microprobe analyses and actual distances, see the data repository.

that defines *Arita's* [1983] MCT I is not exposed at this location. Along this transect, domain 2 rocks were collected between the MCT and the boundary defined by *Colchen et al.* [1980] as the contact between aluminous and carbonate schists of the upper Lesser Himalaya and those of the lower Lesser Himalaya's Kunchha Formation (Plate 2). For reasons discussed in section 9, we correlate this contact with the MCT I (Plates 4 and 5a). We arbitrarily assign this boundary as the contact between the upper and lower Lesser Himalaya metasediments is unclear [see *Upreti*, 1999].

All rocks sampled contain quartz + ilmenite ± garnet ± muscovite ± plagioclase ± epidote (allanite) ± monazite ± zircon ± tourmaline ± apatite. Domain 3 samples also contain garnet + biotite + chlorite. Garnet may appear in these rocks via a continuous reaction involving chlorite breakdown (chlorite + quartz → garnet + H_2O). One domain 3 sample (MA63) contains chloritoid + biotite.

From domain 3 to domain 2, the rocks follow a systematic temperature and pressure increase. Lower domain 2 samples have garnet + biotite + chlorite, whereas staurolite or kyanite appear in upper structural levels. Staurolite is only seen along the Darondi Khola, whereas kyanite only appears along the Marysandi River transect. Rocks collected in upper structural levels of domain 2 commonly lack plagioclase, and their chlorite appears retrograde, whereas rocks of domain 3 and lower structural levels of domain 2 have prograde chlorite. One domain 2 sample is a graphitic schist (MA79), which contains abundant plagioclase, but no muscovite was found. A sequence of marls, graphitic marls, and quartzites is observed within domain 2, but this paper focuses only on the garnet-bearing assemblages.

Domain 1 samples contain garnet + biotite + chlorite ± kyanite ± sillimanite. Plagioclase is abundant in all domain 1 rocks. Along the Darondi Khola, kyanite was not found. Along the Marysandi River transect, kyanite occurs near the MCT in domains 1 and 2, whereas sillimanite appears in structurally higher levels of domain 1. The appearance of sillimanite is consistent with a pressure decrease via the reaction of kyanite → sillimanite. Sample MA18 contains both kyanite and small mats of fibrolitic sillimanite. Sample MA11, the structurally highest domain 1 sample collected, is a garnet- and tourmaline-bearing, foliated felsic gneiss collected near the possible South Tibetan Detachment near the town of Chame.

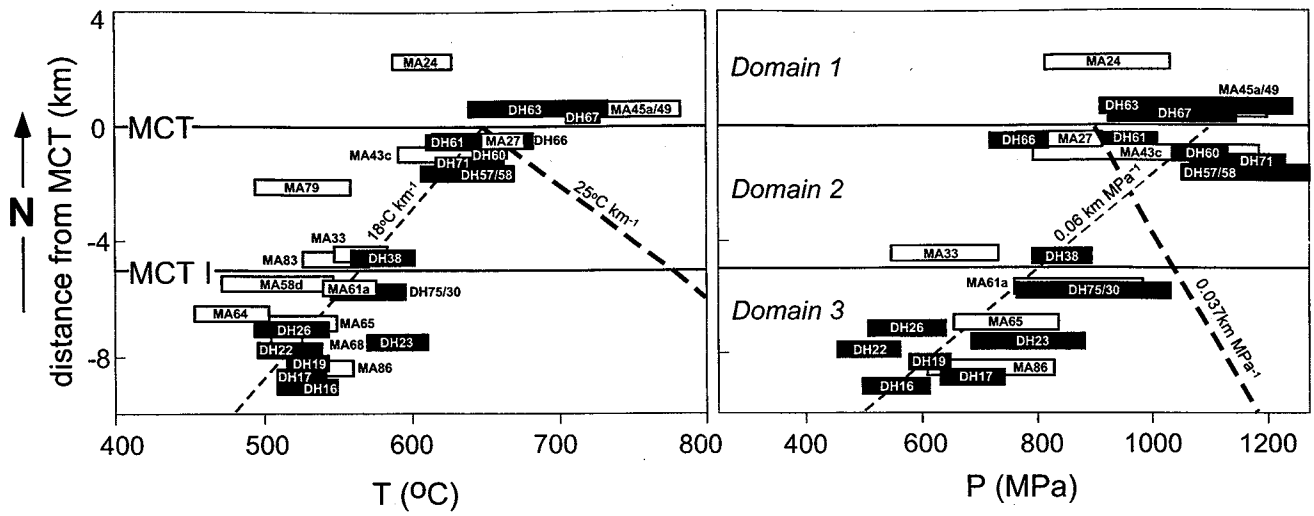

Figure 4. Thermobarometric results from the Darondi Khola and the Marysandi River transects plotted versus structural distance from the MCT. See Plate 9 for these results plotted on a P-T diagram. The temperature within a range of 0-1000 MPa is plotted for samples MA79, MA83, MA64, MA68, and MA58. The width of the symbol indicates uncertainty. Solid boxes are from the Darondi Khola, and open boxes are from the Marysandi River transect. Sample numbers are in or near the boxes. (Left) Temperature data with both the 25°C km^{-1} geotherm (bold dashed line) and an estimated thermal gradient of -18°C km^{-1} (lighter dashed line) indicated. (Right) Pressure data with both the 0.37 km MPa^{-1} lithostatic pressure gradient (bold dashed line) and an estimated pressure gradient of -0.06 km MPa^{-1} (lighter dashed line) indicated. Mineral compositions used to calculate these pressure and temperature conditions are available in the data repository.

6. Thermobarometric Information from Central Nepal Garnet-Bearing Assemblages

Appendix A outlines the methods used to obtain thermobarometric data from the central Nepal samples. For descriptions of the Darondi Khola samples, see also *Kohn and Spear* [2001] and M.J. Kohn et al., P-T-t path discontinuity in the MCT zone, central Nepal, submitted to *Geology*, 2000.

6.1. Garnet X-ray Element Maps

Garnet X-ray element maps from the Greater Himalayan Crystallines (domain 1; Plate 6), upper Lesser Himalaya (domain 2; Plate 7) and lower Lesser Himalaya (domain 3; Plate 8) show striking differences in zoning of Mn, Ca, Mg, and Fe. Compositional traverses across these garnets (Figure 3) indicate the units experienced unique thermal histories [see also *Kohn et al.*, 1999].

6.1.1. Domain 1 samples: Greater Himalayan Crystallines. Lack of noticeable zoning within the interior of most garnets from the Greater Himalayan Crystallines is typical of high-grade metamorphic rocks [e.g., *Tracy et al.*, 1976; *Chakraborty and Ganguly*, 1991; *Florence and Spear*, 1991] and is consistent with that reported from the unit elsewhere in the range [e.g., *Hodges et al.*, 1993; *Metcalfe*, 1993; *Kaneko*, 1995; *Davidson et al.*, 1997]. Plate 6 is an example of a domain 1 garnet and has the mineral assemblage garnet + biotite + chlorite + plagioclase + muscovite + allanite + monazite + ilmenite + quartz. The sample was collected ~2.5 km north of the MCT along the Marysandi River transect (MA49, see Plate 3 for location). The garnet shows a flat zoning profile of 0.050-0.025 mole fraction spessartine, but close to the rim it sharply increases to 0.065 mole fraction (Figure 3). Domain 1 garnets collected near the MCT are unzoned in Fe/(Fe+Mg) and Mn, or show flat profiles in their cores with an increase toward the rims. The behavior suggests that their compositions homogenized via diffusion at high temperature and experienced retrograde garnet resorption during cooling [*Florence and Spear*, 1991].

P-T path calculations were not attempted for domain 1 assemblages because the original metamorphic compositions appear modified [e.g., *Spear and Parish*, 1996]. To estimate their P-T conditions, analyses were obtained from the portion of the garnet that exhibited the lowest Mn and Fe/(Fe+Mg) values, avoiding the retrograde rim. Several analyses of biotite, muscovite, plagioclase, and chlorite were taken both near and far from the garnet to explore their compositional heterogeneity.

6.1.2. Domain 2 samples: Upper Lesser Himalaya Formation. Domain 2 garnets near the MCT have X-ray element maps similar to those of domain 1, whereas those near the MCT I are complexly zoned. For example, Plate 7 shows a garnet from sample MA27, located ~0.2 km below the MCT, and a garnet from sample MA33, collected ~8 km below the MCT. Both rocks are classified within a single lithology [*Colchen et al.*, 1980] and contain garnet + biotite + chlorite + plagioclase + muscovite + allanite + monazite + ilmenite + quartz. The MA27 garnet is affected by diffusion (Figure 3), similar in some ways to the MA49 garnet, whereas MA33 garnet has a distinct zoning profile that spikes sharply in Mn, Fe, and Mg and decreases sharply in Ca within 0.02 mm of the rim. Geochronologic data indicate that the MA33 garnet records a two-stage metamorphic history [*Catlos et al.*, 2000]. Garnets from MA27 show overall lower grossular abundance within their cores and patchy areas of higher Ca at the rims, suggesting that the grains grew during burial. Similar behavior is observed in garnets obtained at equivalent

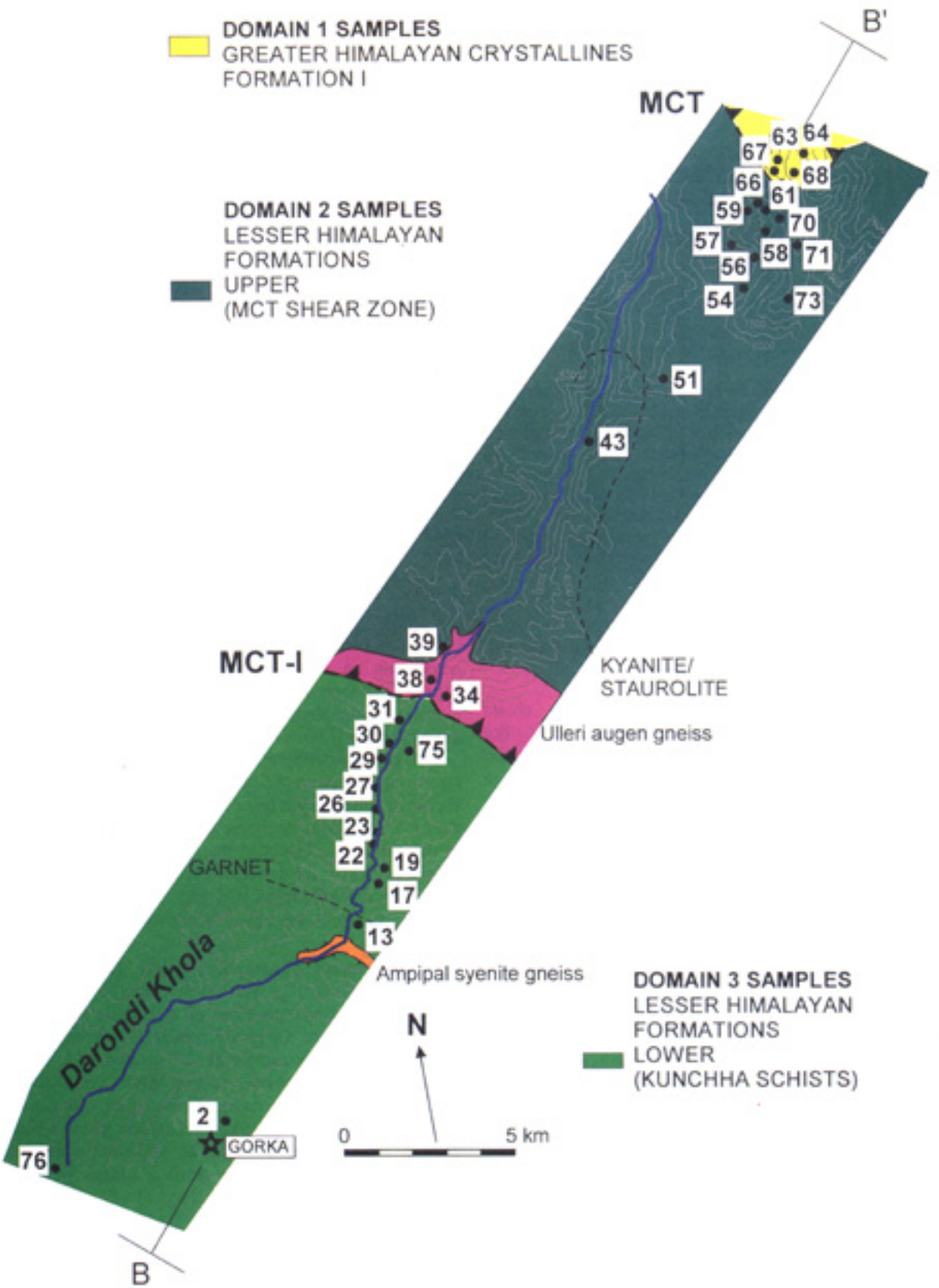

Plate 4. Sample location map from rocks collected along the Darondi Khola. These samples are indicated by "DH" in the text of the paper. Town names are in boxes and designated by stars. Isograds are dashed and labeled. See Plate 5b for the cross section through B-B'.

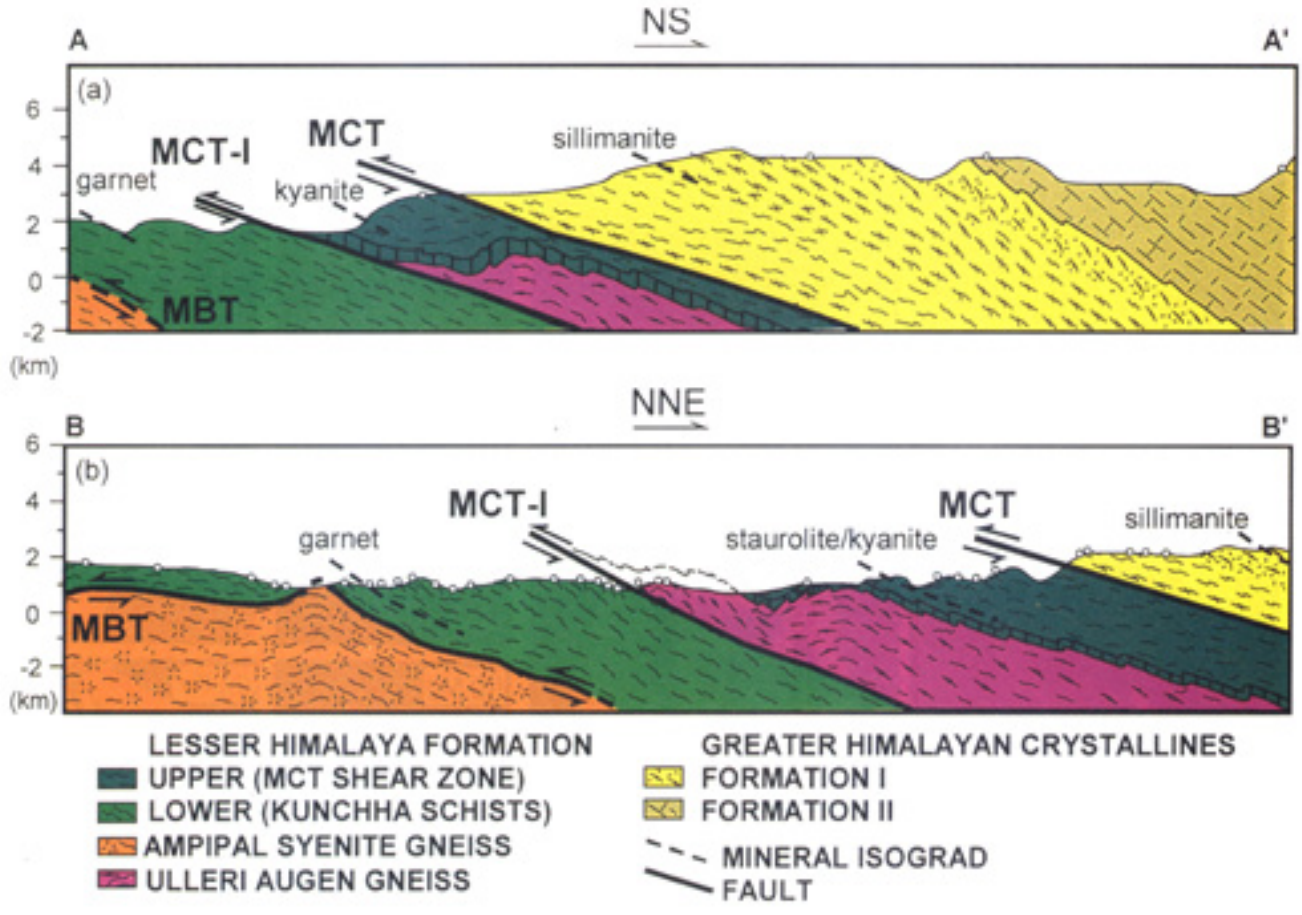

Plate 5. Geologic cross-sections along (a) the Marysandi River and (b) Darondi Khola transects. See Plates 3 and 4 for the traverse locations. These cross sections are not vertically exaggerated.

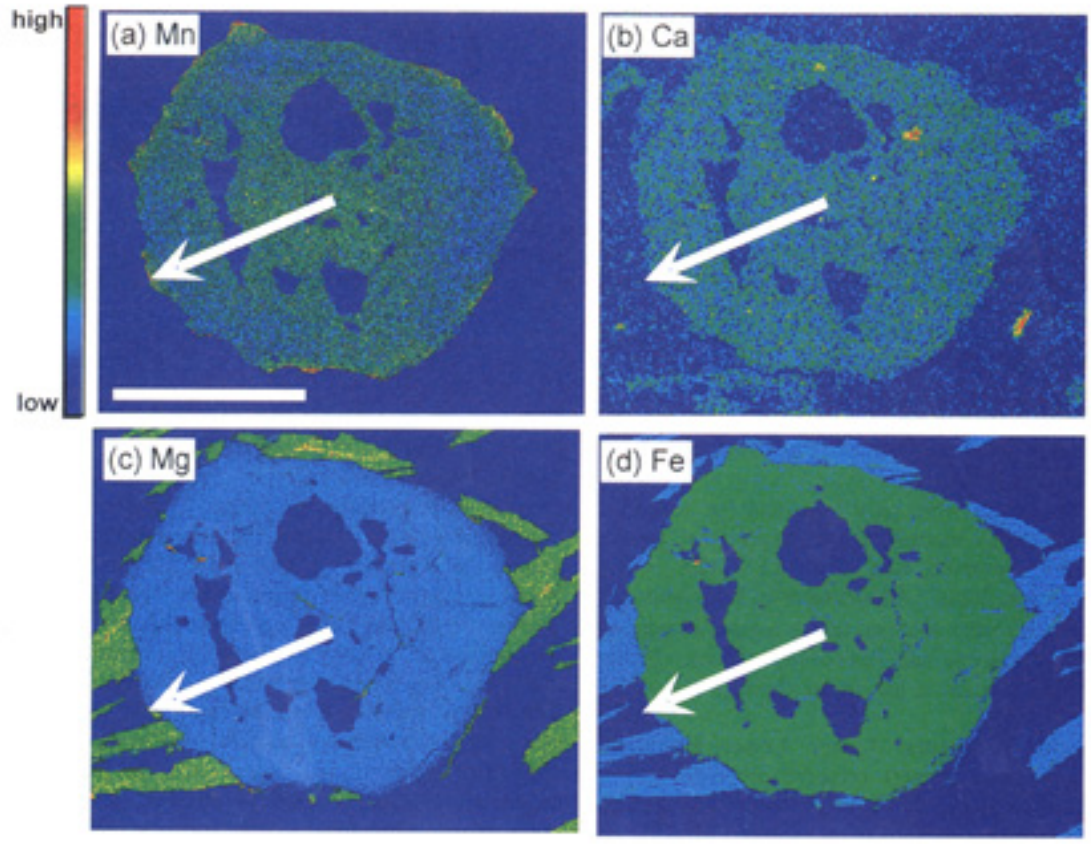

Plate 6. Electron microprobe X-ray element maps of (a) Mn, (b) Ca, (c) Mg, and (d) Fe for domain 1 garnet MA49. See Plate 3 for sample location. Compositions along the white arrow are shown in Figure 3. The scale bar is 500 μm.

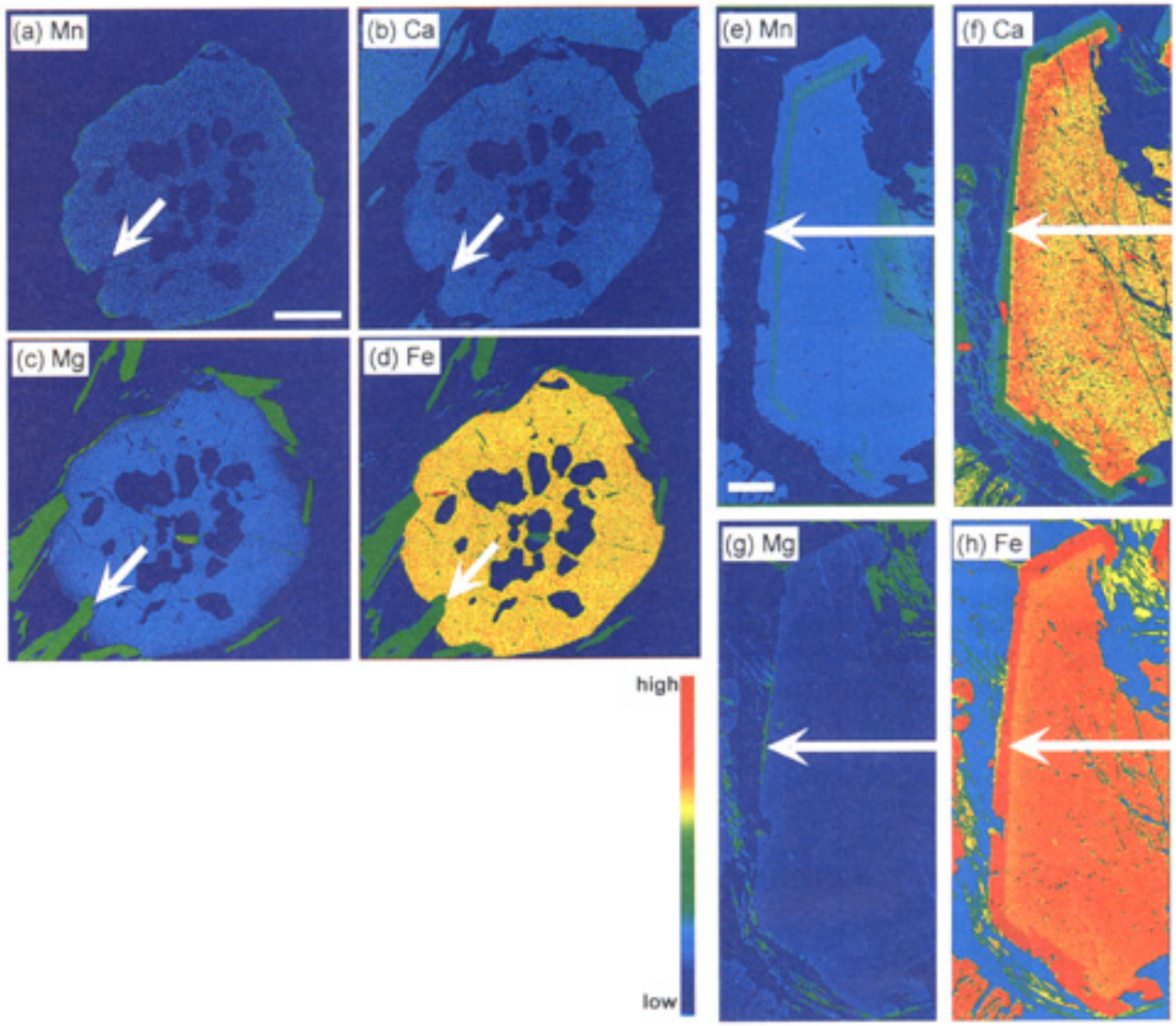

Plate 7. (a-d) Electron microprobe X-ray element maps of Mn, Ca, Mg, and Fe for domain 2 garnet MA27. (e-h) Electron microprobe X-ray element maps of Mn, Ca, Mg, and Fe for half of domain 2 garnet MA33. See Plate 3 for sample locations. Compositions along the white arrows are shown in Figure 3. The scale bar is 500 μm.

structural locations (MA81) but is contrary to the higher Ca cores seen in domain 1 and structurally lower domain 2 samples (MA43, MA33, MA83).

P-T path calculations were only estimated for domain 2 garnets in which X-ray element maps suggest that growth compositions are preserved (see also M.J. Kohn et al., submitted manuscript, 2000). All estimates of P-T conditions for domain 2 samples were obtained on the regions of garnets with the lowest spessartine and Fe/(Fe+Mg) values. In the case of MA33 this location is just inside the rim, outside of the Mn spike.

6.1.3. Domain 3 samples: Lower Lesser Himalaya Formation. Domain 3 garnets preserve prograde zoning patterns and signal an abrupt shift from those characterized by significant retrogression (domain 1 garnet MA49) or complicated histories (domain 2 garnet MA33). For example, Plate 8 shows an example of a domain 3 garnet from sample MA61 collected ~2 km south of the MCT I (see Plate 3 for sample location). This rock contains garnet + biotite + chlorite + plagioclase + apatite + allanite + ilmenite + tourmaline + quartz. Ca-rich inclusions in Plate 8 are allanite grains, the dominant accessory mineral in the rock. The MA61 garnet decreases in spessartine and Fe/(Fe+Mg) from core to rim (Figure 3), as expected if it grew with increasing temperature and preserved changing compositions [*Spear et al.*, 1990]. The rounded garnet is mantled by chlorite, but the lack of Mn or Fe/(Fe+Mg) increase at the rim suggests the effect of resorption is minimal. The garnet shows a concentric compositional pattern with the exception of the upper right quadrant, where it is truncated, suggesting that the grain broke subsequent to the formation of zoning. To estimate the peak metamorphic conditions, the garnet's lowest

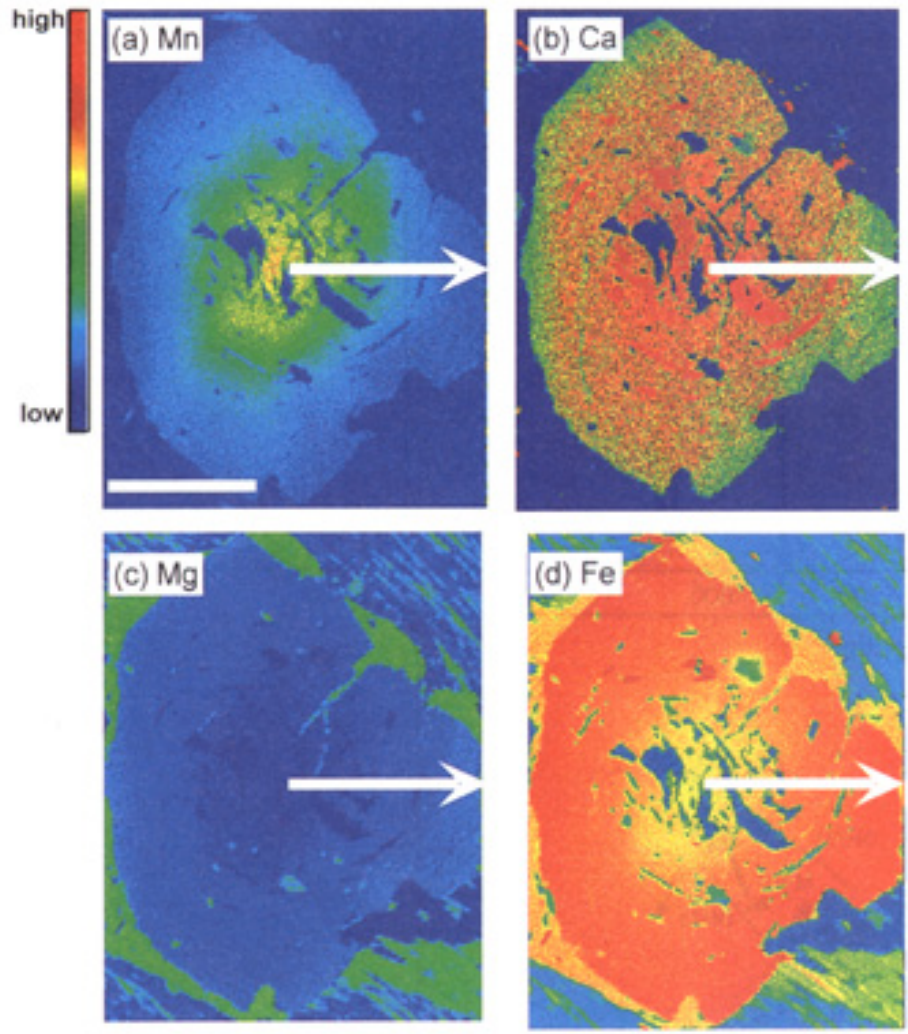

Plate 8. Electron-microprobe X-ray element maps of (a) Mn, (b) Ca, (c) Mg, and (d) Fe for domain 3 garnet MA61. See Plate 3 for sample location. Compositions along the white arrow are shown in Figure 3. The scale bar is 500 μm.

Mn and Fe/(Fe+Mg) compositions were used. As done with domain 1 and 2 samples, the heterogeneity of the minerals used for thermobarometry was explored.

6.2. Thermobarometry

Figure 4 summarizes the minimum P-T conditions recorded by samples collected in central Nepal. Only temperature is calculated for some samples (MA79, MA83, MA64, MA68, MA58), and is plotted within 0-1 GPa in Figure 4. Plate 9 displays the P-T paths recorded by garnets that display prograde zoning patterns.

6.2.1. Peak metamorphic P-T estimates. Many Himalayan rocks show evidence of ReNTRs [see M.J. Kohn et al., submitted manuscript, 2000; *Kohn and Spear*, 2001]. Evidence to support the pressures and temperatures reported for the samples analyzed here is that the estimated conditions agree with (1) the observed mineral assemblages, (2) absence of partial-melting textures, and (3) P-T conditions of other assemblages collected nearby.

Domain 1 rocks yield the highest temperatures and pressures of 600-800°C and 0.8-1.3 GPa (Figure 4 and Plate 9), similar to data reported from Greater Himalayan Crystallines rocks from the Garhwal Himalaya, central Nepal, and the Bhutan Himalaya [*Hodges et al.*, 1993; *Metcalfe*, 1993; *Kaneko*, 1995; *Davidson et al.*, 1997]. The high-grade metamorphic conditions recorded by domain 1 samples collected near the MCT may reflect their exhumation from greater depths along the MCT ramp, or the Eohimalayan event, when unit was buried beneath the southern edge of Tibet.

Domain 2 samples collected near the MCT yield higher or similar peak pressure and temperature results as those from domain 1, whereas those collected near the MCT I yield lower estimates (Figure 4 and Plate 9). Samples from domain 3 reveal the lowest temperatures and pressures of ~550°C and ~0.6-0.7 GPa. The footwall increases in both temperature and pressure toward the fault from domains 3 to 2. Figure 4 shows an apparent thermal gradient (~18°C km^{-1}) and pressure gradient (~0.06 km MPa^{-1}) are inverted and differ from lithostatic values (25°C km^{-1}, 0.037 km MPa^{-1}).

6.2.2. P-T paths. Table 1 shows the mineral compositions used to obtain the P-T paths. All central Nepal garnets analyzed here grew with increasing temperature (Plate 9).

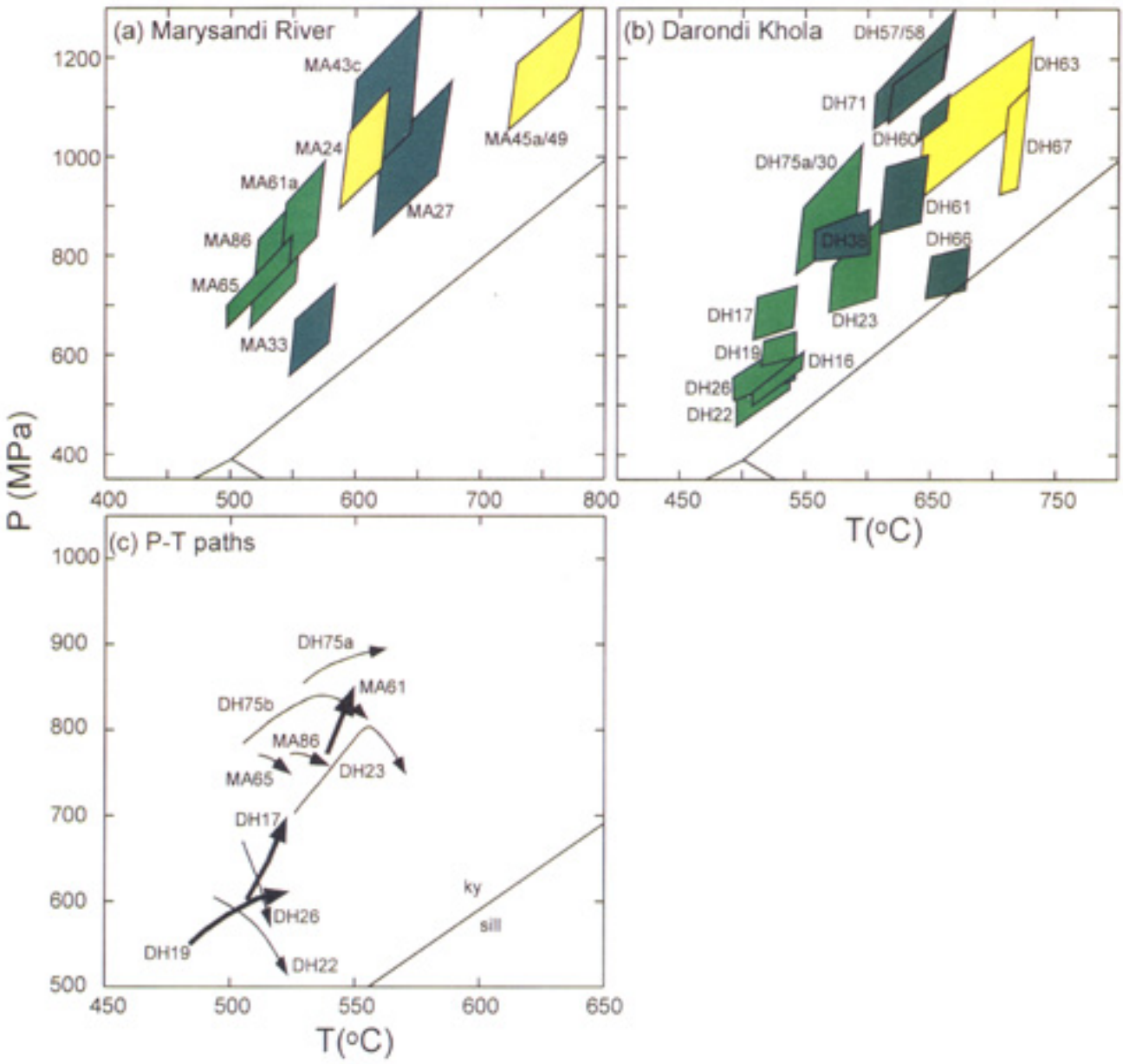

Plate 9. Metamorphic pressures and temperatures calculated for domain 2 and 3 garnet-bearing assemblages collected along the (a) Marysandi River and (b) Darondi Khola transects. (c) P-T paths for Darondi Khola and Marysandi River transect garnet-bearing assemblages. Paths from structurally lower domain 3 samples that show garnet growth with increasing pressure and temperature are indicated with a bold line. See Table 1 and the data repository for the mineral compositions used to calculate these conditions.

Some record little change in pressure (DH75a) or decrease in pressure with increasing temperature (MA65, MA86, DH26, DH23, DH26, DH22), consistent with heating during exhumation (Figure 1). Structurally lower garnets (MA61, DH17, DH19) grew during an increase in both pressure and temperature. The change in path suggests a structural and metamorphic discontinuity exists within the MCT footwall, far south of the mapped lithologic (~2 km [*Colchen et al.*, 1980]) and tectonic breaks (~5 km [*Arita*, 1983]). The disparate P-T paths are 2 point core-rim paths and are strongly dependent on the composition of plagioclase within the rocks. To establish their validity, to explore their significance, and to link the thermobarometric results with a temporal history, in situ monazite Th-Pb ages and $^{40}Ar/^{39}Ar$ muscovite ages were obtained.

7. Th-Pb Ion Microprobe Analyses of Monazite

Petrologic observations suggest monazite appears in pelites via allanite breakdown at ~525°C [*Smith and Barriero*, 1990; *Kingsbury et al.*, 1993; *Wing et al.*, 1999]. Monazite preferentially incorporates ThO_2 [e.g., *Overstreet*, 1967] but sustains little radiation damage upon annealing [e.g., *Meldrum et al.*, 1998] and remains closed to Pb loss at relatively high temperatures (600-650°C [*Smith and Giletti*, 1997]). When

Table 1. Mineral Compositions Used for P-T Path Modeling

Sample[a]	X_{alm}[b]	X_{sps}[c]	X_{grs}[d]	X_{an}[e]	Source[f]
MA61	0.751	0.016	0.169	0.21	rim
	0.643	0.098	0.216	0.27	core
MA65	0.793	0.048	0.095	0.15	rim
	0.708	0.101	0.141	0.16	core
MA86	0.791	0.040	0.103	0.14	rim
	0.688	0.087	0.173	0.18	core
DH17	0.774	0.092	0.070	0.13	rim
	0.684	0.149	0.119	0.23	core
DH19	0.788	0.039	0.110	0.23	rim
	0.608	0.188	0.170	0.26	core
DH22	0.807	0.060	0.065	0.19	rim
	0.692	0.147	0.115	0.19	core
DH26	0.713	0.158	0.048	0.13	rim
	0.682	0.175	0.070	0.13	core
DH23	0.783	0.045	0.099	0.20	rim
	0.732	0.058	0.151	0.20	
	0.164	0.036	0.631	0.22	core
DH75a	0.771	0.006	0.135	0.19	rim
	0.764	0.010	0.165	0.19	
	0.693	0.067	0.199	0.21	core
DH75b	0.751	0.016	0.084	0.20	rim
	0.729	0.037	0.132	0.20	
	0.612	0.157	0.167	0.21	core

[a]MA, Marysandi River sample, DH, Darondi Khola sample. See Plates 3 and 4 for sample locations. See Plate 9 for these P-T paths. All rocks were modeled using Progam Gibbs, version 4.7 [*Spear et al.*, 1997], with the observed assemblage garnet + biotite + chlorite + muscovite + plagioclase + quartz in the MnNCKFMASH system. See Appendix B and the data repository for further details. Data for the Darondi Khola transect reported by M.J. Kohn et al. (submitted manuscript, 2000).

[b]X_{alm}, mole fraction almandine.

[c]X_{sps}, mole fraction spessartine.

[d]X_{grs}, mole fraction grossular.

[e]X_{an}, mole fraction anorthite. Plagioclase composition changes were constrained from only matrix grains.

[f]Compositions from the rim and core, respectively, from the sample. For some samples an intermediate point was also used in the P-T path calculations.

encompassed by garnet, the low solubility and permeability of Pb in the host armor monazite against daughter product loss [*Montel et al.*, 2000]. In multiply metamorphosed terranes, monazite may lose Pb via diffusion or a dissolution-precipitation process [*Kingsbury et al.*, 1993; *Ayers et al.*, 1999; *Montel*, 1999]. In central Nepal, allanite is the dominant rare earth bearing accessory mineral within the chlorite and biotite zones. Above the garnet isograd, no readily apparent correlation exists between the presence of allanite or monazite with metamorphic grade.

Monazite grains were analyzed from samples collected from domain 1 (Figure 5), domain 2 (Figure 6) and domain 3 (Figures 7 and 8) along the Marysandi River and Darondi Khola. Appendix B outlines the methods used to obtain the ages. Tables 2 and 3 and Plates 10-12 summarize the geochronologic data along both transects. The uncertainty in all ages reported here is at the 1σ level.

7.1. Domain 1 Samples: Greater Himalayan Crystallines

Domain 1 monazite grains yield a range of ages, consistent with Oligocene formation followed by diffusional Pb loss or recrystallization. For example, Figure 5 is a BSE image of sample MA45 (P ≈ 1 GPa; T ≈ 735°C). In this sample, monazite ages range from a maximum of 37.5±0.3 Ma for an inclusion in garnet to a significantly younger age of 11.0±0.4 Ma for a matrix grain. The oldest Oligocene ages may represent monazite growth during Eohimalayan metamorphism, whereas the younger are matrix crystals that either recrystallized or continued to experience diffusional reequilibration after the garnet inclusion closed to Pb loss. The ~11 Ma grain is found in a reaction zone around the garnet, and requires ~70% ^{208}Pb loss if it was initially ~34 Ma. Calculations by *Smith and Giletti* [1997] indicate this amount of ^{208}Pb loss is possible if a 50-μm grain was held at ~735°C for 1 Ma. Diffusive Pb loss from domain 1 matrix monazite is further supported by depth profiling measurements of grains from sample DH68 that reveal diffusion profiles within ~2 μm of their surfaces [*Grove and Harrison*, 1999].

7.2. Domain 2 Samples: Upper Lesser Himalaya Formation

Miocene monazite ages characterize rocks immediately beneath the MCT along both drainages, consistent with evidence of activity during this time [e.g., *Hodges et al.*, 1992; *Coleman*, 1998]. For example, monazite in sample MA27 is 18±1 Ma, and samples DH58 and DH71 contain ~22 Ma monazite grains.

Moving south of the MCT, ages decrease from 10-15 Ma to 7-8 Ma (see Plates 10-12). Four domain 2 rocks collected near the lower boundary contain monazite that appear to have formed during the late Miocene (Figure 6). In sample MA83 (T ≈ 545°C), two spots on a monazite inclusion in garnet and four spots on two matrix grains average 8.3±0.5 Ma. In this rock the monazite inclusion in garnet is older than those in the matrix. A late Miocene matrix monazite grain in sample MA33 (P ≈ 0.65 GPa; T ≈ 560°C) is located in an area where garnet was resorbed and could have once been an inclusion. Plate 7 shows the zoning pattern of a garnet in this sample. Late Miocene monazite inclusions are only found in the matrix or within 0.2 mm of the rim (near the area taken for composition), whereas allanite grains are found within the core. *Catlos et al.* [2000] report an allanite found the core of this garnet is significantly older (~270 Ma) than the monazite grains in the rim (~7 Ma). The zoning pattern and the ages of monazite and allanite grains strongly imply this garnet has experienced a two-stage history.

7.3. Domain 3 Samples: Lower Lesser Himalaya Formation

Figure 7 is BSE image of domain 3 sample MA84, collected beneath the MCT I along the Marysandi River transect (for sample location, see Plate 3). This rock records multiple stages of monazite growth and contains a 1.6 Ga monazite grain located <0.5 mm from a ~7 Ma monazite. The oldest grain is large (~70 μm), and the youngest grain is found in an area of the rock that appears strongly foliated. The Proterozoic age is consistent with the assembly of the Indian continent [e.g., *Balasubramaniyam et al.*, 1978], whereas the late Miocene age is interpreted to record footwall crystallization associated with slip within the MCT shear zone. The hypothesis is supported by temperature estimates from sample MA83 (T ≈ 545°C), collected <0.2 km above

Table 2. Th-Pb Ages (±σ) of Spots on Central Nepal Monazite Grains

mon-sp[a]	Age[b], Ma (±σ)
Domain 1 (Fm. II) MA11	
1-1	51.4 (5.2)
3-1	46.6 (4.4)
5-1	28.9 (1.6)
6-1	37.6 (3.8)

Domain 1 (Fm. I)

MA15		MA18		MA 19		MA25		MA45		MA48	
mon-sp	Age, Ma (±σ)	mon-sp	Age, Ma (±σ)	mon-sp	Age, Ma (±σ)	mon-sp	Age, Ma (±σ)	mon-sp	Age, Ma (±σ)	mon-sp	Age, Ma (±σ)
1-1	22.4 (0.6)	1-1	23.2 (0.5)	1-1	20.7 (1.9)	1-1	16.8 (0.9)	1-1	28.3 (0.2)	30-1[c]	29.2 (0.5)
2-1	23.1 (0.9)	2-1	14.1 (0.6)	1-2	20.8 (1.4)	1-2	14.7 (1.0)	1-2	27.6 (0.3)	30-2[c]	26.1 (0.6)
2-2	24.2 (0.8)	3-1	18.7 (0.2)	1-3	18.6 (0.5)	2-1	14.8 (1.1)	1-3	20.5 (0.1)	31-1[c]	18.5 (0.5)
3-1	33.1 (4.8)	4-1	36.5 (0.3)	2-1	23.9 (2.0)	3-1	10.8 (1.8)	1-4	27.9 (0.2)	31-2[c]	6.3 (0.3)
6-1	33.8 (5.0)	5-1	19.5 (0.3)	3-1	24.9 (2.6)	4-1	15.8 (0.9)	1-5	29.4 (0.2)		
7-1	34.8 (6.3)	6-1	28.6 (0.9)	3-2	18.8 (0.7)	4-2	10.7 (0.9)	2-1[c]	37.5 (0.3)		
7-2	37.5 (7.9)			5-1	17.1 (0.7)	5-1	15.9 (0.9)	2-2[c]	30.4 (0.5)		
8-1	27.5 (1.7)			5-2	19.3 (0.7)			4-1	11.0 (0.4)		
								4-2	11.4 (0.2)		

Domain 2

MA27		MA33		MA83		DH58		DH71		DH73		DH51		DH39	
mon-sp	Age, Ma (±σ)	mon-sp	Age, Ma (±σ)	mon-sp	Age, Ma (±σ)	mon-sp	Age, Ma (±σ)	mon-sp	Age, Ma (±σ)	mon-sp	Age, Ma (±σ)	mon-sp	Age, Ma (±σ)	mon-sp	Age, Ma (±σ)
1-1	18.3 (0.6)	1-1[c]	7.0 (0.4)	76-1	8.0 (0.4)	5a-1	21.6 (1.5)	68-1[c]	21.1 (0.8)	72-1[c]	11.9 (0.6)	108-1	10.6 (1.2)	130-1	9.8 (1.3)
1-2	15.3 (1.1)	2-1.	6.7 (0.1)	76-2	7.5 (0.6)	5a-2	366 (21)	67-1[c]	21.7 (1.2)	73-1[c]	14.6 (1.5)	111-1	9.9 (1.2)	123e-1	9.8 (1.6)
1-3	18.7 (0.6)	3-1[c]	6.3 (0.4)	77-1	7.9 (0.6)					73-2[c]	11.9 (0.4)	109-1	9.2 (1.8)	123d-1	8.2 (0.9)
1-4	18.3 (0.6)			77-2	7.9 (0.6)							110-1	10.6 (0.4)		
				87-1[c]	9.5 (0.8)							112a-1	9.4 (1.1)		
				87-2[c]	8.8 (0.6)							113-1	10.1 (2.7)		

Domain 3

MA84		MA65		MA86		DH30		DH75B	
mon-sp	Age, Ma (±σ)	mon-sp	Age, Ma (±σ)	mon-sp	Age, Ma (±σ)	mon-sp	Age, Ma (±σ)	mon-sp	Age, Ma (±σ)
1-1	92.1 (2.3)	1-1	13.5 (1.0)	4-1	2.22 (1.56)	84-1[c]	7.8 (0.9)	79-1[c]	7.6 (0.2)
2-1	321 (17)	2-1	11.7 (0.5)	4-2	3.43 (0.76)	87-1	7.7 (0.4)	78-1[c]	7.8 (0.2)
5-1	7.8 (0.5)	4-1	15.5 (1.4)	4-3	4.16 (1.11)	87-2	6.9 (0.5)	77-1[c]	10.3 (0.9)
6-1	1674 (15)	6-1	15.7 (0.6)	4-4	3.50 (0.18)	6-1[c]	8.9 (0.7)	82-1[c]	11.1 (0.7)
6-2	1696 (40)	7-1	10.5 (0.7)	4-5	3.36 (0.17)	7-1[c]	9.3 (0.5)		
		9-1	9.5 (0.4)	1-1	2.88 (0.15)	86-1	7.8 (0.7)		
		11-1	20.4 (1.0)	2-1	3.13 (0.97)				
				1-1	3.41 (0.50)				
				1b-1	4.88 (1.44)				
				2-1	2.90 (0.87)				
				7-1	3.64 (1.34)				
				7a-1	3.82 (0.55)				
				6-1	6.01 (1.21)				

[a]The nomenclature indicates the grain and spot, respectively, of the analyzed monazite. MA, Marysandi River sample; DH, Darondi Khola sample. See Plates 3 and 4 for locations. Domain 1, Greater Himalayan Crystallines; Fm. I and Fm. II, Greater Himalayan Crystallines Formations I and II of *Colchen et al.* [1980]; domain 2, upper Lesser Himalaya; domain 3, lower Lesser Himalaya.
[b]Spot age (±1σ).
[c]Monazite inclusion in garnet.

Table 3. Summary of Muscovite $^{40}Ar/^{39}Ar$ Analyses

Sample[a]	Total Gas Age, Ma (±1σ)	($^{40}Ar/^{36}Ar$)atm[b] (±1σ)	MSWD[c]
	Domain 1		
DH64	4.37 (0.08)	291.5 (37.4)	2.4
DH68	13.9 (0.08)	448.4 (92.5)	5843
	Domain 2		
DH66	5.74 (0.05)	289.4 (22.7)	13
DH70b[d]	2.84 (0.05)	273.2 (40.3)	78
DH57	3.27 (0.06)	299.4 (77.1)	1.5
DH54[d]	2.64 (0.04)	293.3 (8.6)	3.3
DH51[d]	2.80 (0.31)	337.8 (51.4)	0.3
DH43[d]	3.43 (0.30)	295.9 (25.4)	1.8
DH39	6.28 (0.03)	427.4 (109.6)	171
DH34	9.15 (0.10)	319.5 (94.9)	63
DH70a	5.18 (0.06)	350.9 (87.4)	298
DH56	15.9 (0.3)	-1754 (4400)	364
DH59[d]	7.9 (0.6)	347.2 (127.8)	5.4
	Domain 3		
DH31	4.85 (0.04)	317.5 (19.1)	13
DH29	14.5 (0.1)	3226 (11655)	1770
DH27	12.1 (0.1)	432.9 (99.3)	102
DH17	12.3 (0.6)	304.0 (41.6)	7.4
DH13	36.8 (0.1)	2439 (9340)	2718
DH2	116.8 (0.5)	-302.1 (230.9)	3013
DH76	257 (1)	-4348 (2079)	17768

[a]Darondi Khola samples. See Plate 4 for locations. Domain 1, Greater Himalayan Crystallines; domain 2, upper Lesser Himalaya; domain 3, lower Lesser Himalaya.
[b]($^{40}Ar/^{36}Ar$)atm, ratio in sample that represents the isotopic composition found in present-day atmosphere.
[c]Mean square weighted deviation. See the data repository for numerical results, age spectra, and isochron plots.
[d]Calculations exclude the last step in the heating program.

MA84, which is inconsistent with diffusive Pb loss from a ~0.1 mm-sized monazite [*Smith and Giletti*, 1997]. Smaller (<40 μm) MA84 monazite grains yield Carboniferous and Cretaceous ages, indicating either multiple growth stages or Pb loss. The Carboniferous age may time the ~500 Ma Pan African event [e.g., *Le Fort et al.*, 1986], coupled with Pb loss, but the Cretaceous age has no known corollary. The material needed to form the late Miocene monazite may originate from the dissolution of these grains.

Sample MA65 (P ≈ 0.75 GPa; T ≈ 510°C) contains matrix monazite grains that range from 20±1 Ma to 9.5±0.4 Ma and yields a weighted mean age of 12.1±0.2 Ma. Older ages may represent artifacts of larger amounts of common Pb (the grains are 94±5% $^{208}Pb^*$) or monazite growth due to Miocene MCT slip. These grains probably failed to fully reset during late Miocene MCT-related activity due to the lower P-T conditions experienced by the rock. These ages lead us to suspect that this sample represents a structurally lower domain 2 sample, because the rock was collected ~2 km west of the main Marysandi River transect and its structural distance from the base of the Greater Himalayan Crystallines is speculative.

Figure 8 shows BSE images of sample MA86 (P ≈ 0.72 GPa; T ≈ 535°C), collected near the garnet isograd, which contains some of the youngest monazite grains dated in this study. MA86 monazites yield a weighted mean age of 3.3±0.1 Ma. The 0.1-mm-sized grains are not found as inclusions in garnet, but near or within biotite grains that crosscut the fabric of the rock. High-contrast BSE images

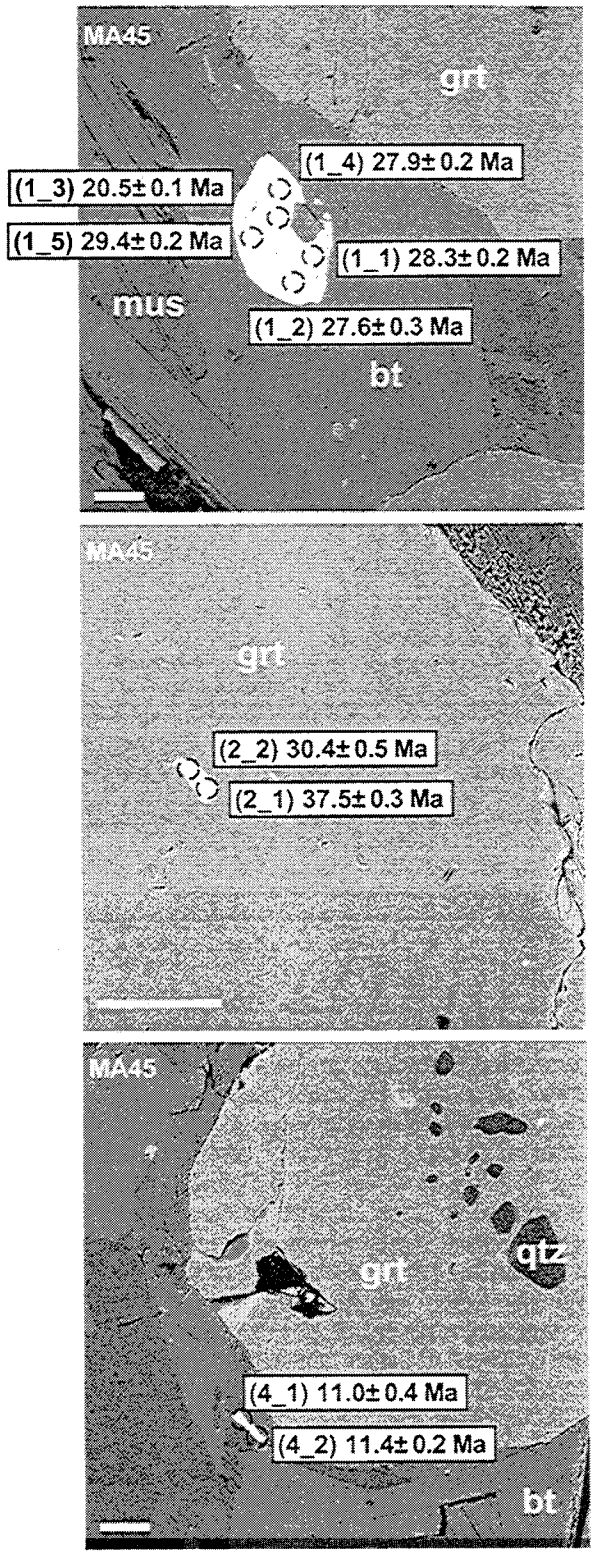

Figure 5. BSE images of domain 1 sample MA45 with age information (1σ) indicated. The scale bar is 100 μm. mus, muscovite; grt, garnet; bt, biotite; qtz, qūartz. Details regarding the analyses are available in the data repository.

reveal no zoning within these grains. The ages from sample MA86 indicates this portion of the MCT shear zone continued activity until at least the Pliocene. Unfortunately, attempts to date other domain 3 monazites were unsuccessful (MA64, MA74, MA71, DH16, DH19) because these grains contained large amounts of common Pb.

8. Muscovite $^{40}Ar/^{39}Ar$ Ages

Himalayan micas typically yield ages affected by extraneous argon, [e.g., *Coleman and Hodges*, 1996; *Vannay and Hodges*, 1996], and several samples analyzed here yield poorly-correlated arrays of $^{39}Ar/^{40}Ar$ versus $^{36}Ar/^{40}Ar$. (Details of the muscovite analyses are available at http://oro.ess.ucla.edu/argonlab/data_repositiory.html.) See Appendix C for a brief summary of the $^{40}Ar/^{39}Ar$ dating methods.

Table 3 summarizes muscovite $^{40}Ar/^{39}Ar$ measurements. Muscovites that contain uniformly distributed $^{40}Ar^*$ produced in situ and a trapped atmospheric component of $^{40}Ar/^{36}Ar$ of ~295.5 represent cooling through the muscovite closure temperature, generally ascribed to be ~350°C [*Purdy and Jäger*, 1976; *Jäger*, 1979]. Muscovites showing poor correlation between $^{39}Ar/^{40}Ar$ versus $^{36}Ar/^{40}Ar$ and nonatmospheric trapped $^{40}Ar/^{36}Ar$ values generally contain extraneous argon and their ages can be difficult to interpret.

Twelve samples collected along the Darondi Khola transect yield late Miocene and Pliocene total gas ages, similar to the youngest mica ages reported from the Marysandi River (Plate 10) [*Edwards*, 1995]. Plate 11 summarizes the geochronologic information obtained along the Darondi Khola. Pliocene mica ages extend from ~8 km north of the MCT along the Marysandi River transect (4.6±0.1 Ma [*Edwards*, 1995]) to the base of the Ulleri augen gneiss along the Darondi Khola transect (4.85±0.04 Ma). The oldest micas analyzed in this study are the structurally lowest samples DH2 (116.8±0.2 Ma) and DH76 (257±1 Ma).

9. Discussion

9.1. Thermobarometry

Garnet elemental zoning patterns and thermobarometric information indicate samples from domain 1 (Greater Himalayan Crystallines) and domain 2 (upper Lesser Himalaya) experienced significantly different reaction and/or P-T histories than those of domain 3 (lower Lesser Himalaya). Garnets from domain 1 and upper levels of domain 2 appear to lose their original compositional zonation via diffusion, whereas garnets from domain 3 and lower structural levels of domain 2 preserve much of their original elemental distributions.

Thermobarometry for footwall rocks reveals an apparent inverted thermal gradient of ~18°C km^{-1} and apparent pressure gradient of ~0.06 km MPa^{-1} (Figure 4). All footwall garnets grew with increasing temperature, and most record P-T paths consistent with the one-slip model and heating during exhumation (Figure 1 and Plate 9). Garnets in samples MA61, DH19, and DH17 grew with increasing pressure, indicating the presence of a metamorphic break north of the garnet isograd along the Darondi Khola and Marysandi River transects. The presence of a tectonic discontinuity within structurally lower levels of the MCT footwall is consistent with a multislip model (Figure 2).

Samples DH17, DH19, and MA61 record fundamentally different P-T paths than other rocks collected along the transects that show decompression. P-T paths are strongly dependent on the methods used in their calculation, including

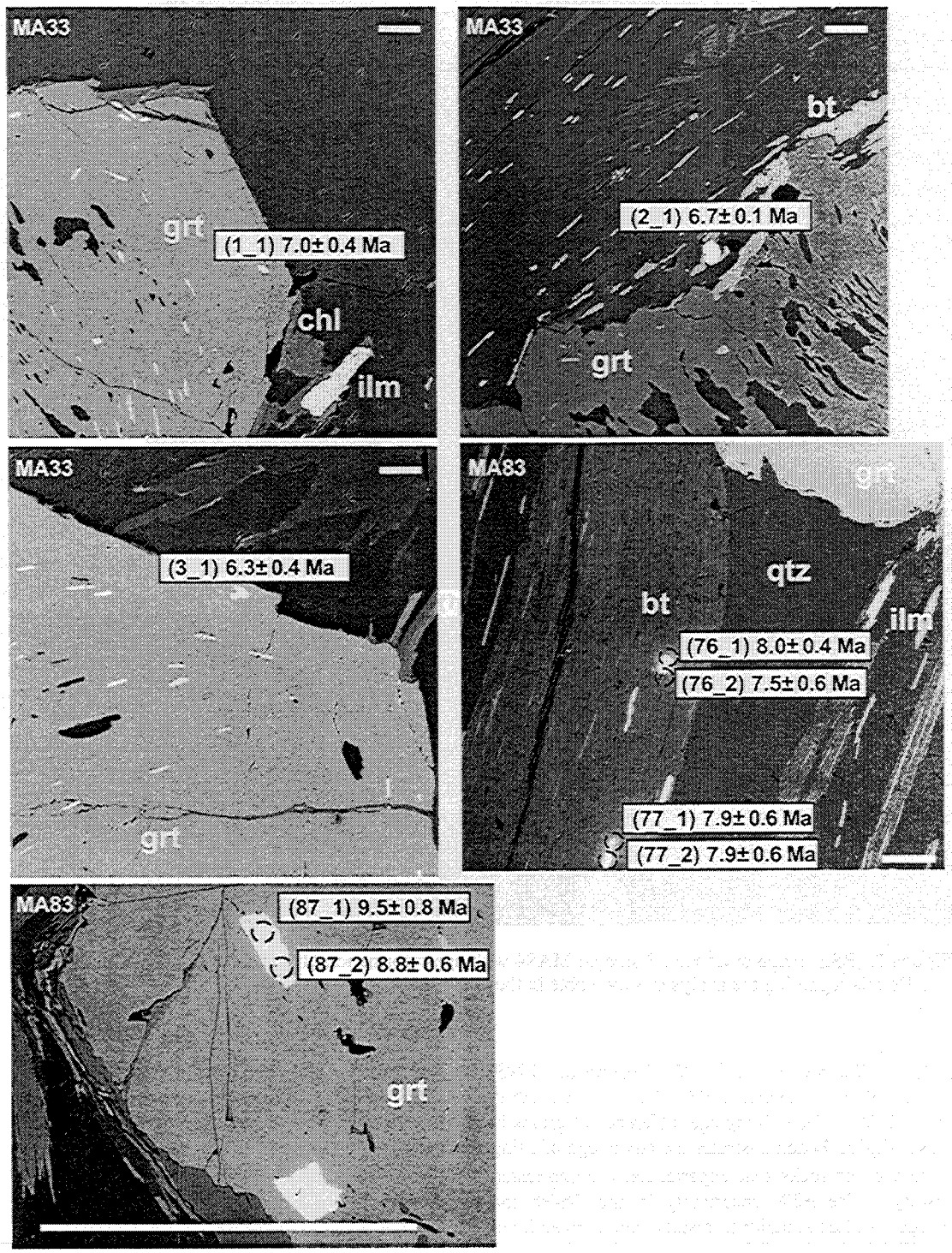

Figure 6. BSE images of domain 2 samples MA33 and MA83 with age information (1σ) indicated. The sample number is indicated in the top left corner of the image. See Plate 7 for X-ray element maps and electron microprobe compositional information for the MA33 garnet. The scale bar is 100 μm. chl, chlorite; ilm, ilmenite; grt, garnet; bt, biotite. Details regarding the analyses are available in the data repository.

assumptions about the rock's assemblage and mineral zoning. The ability to evaluate the thermobarometric results is possible by obtaining the temporal history of the sample. In this case, rocks with disparate P-T paths are near samples that contain late Miocene and Pliocene monazite grains and further support a multislip model.

9.2. Geochronology

The ion microprobe permits in situ microanalysis of radiogenic element-bearing minerals in polished rock thin sections [e.g., *Hinton*, 1995]. Our methods to obtain information about the deformation history of the Himalaya differ from those attempted previously that required mineral

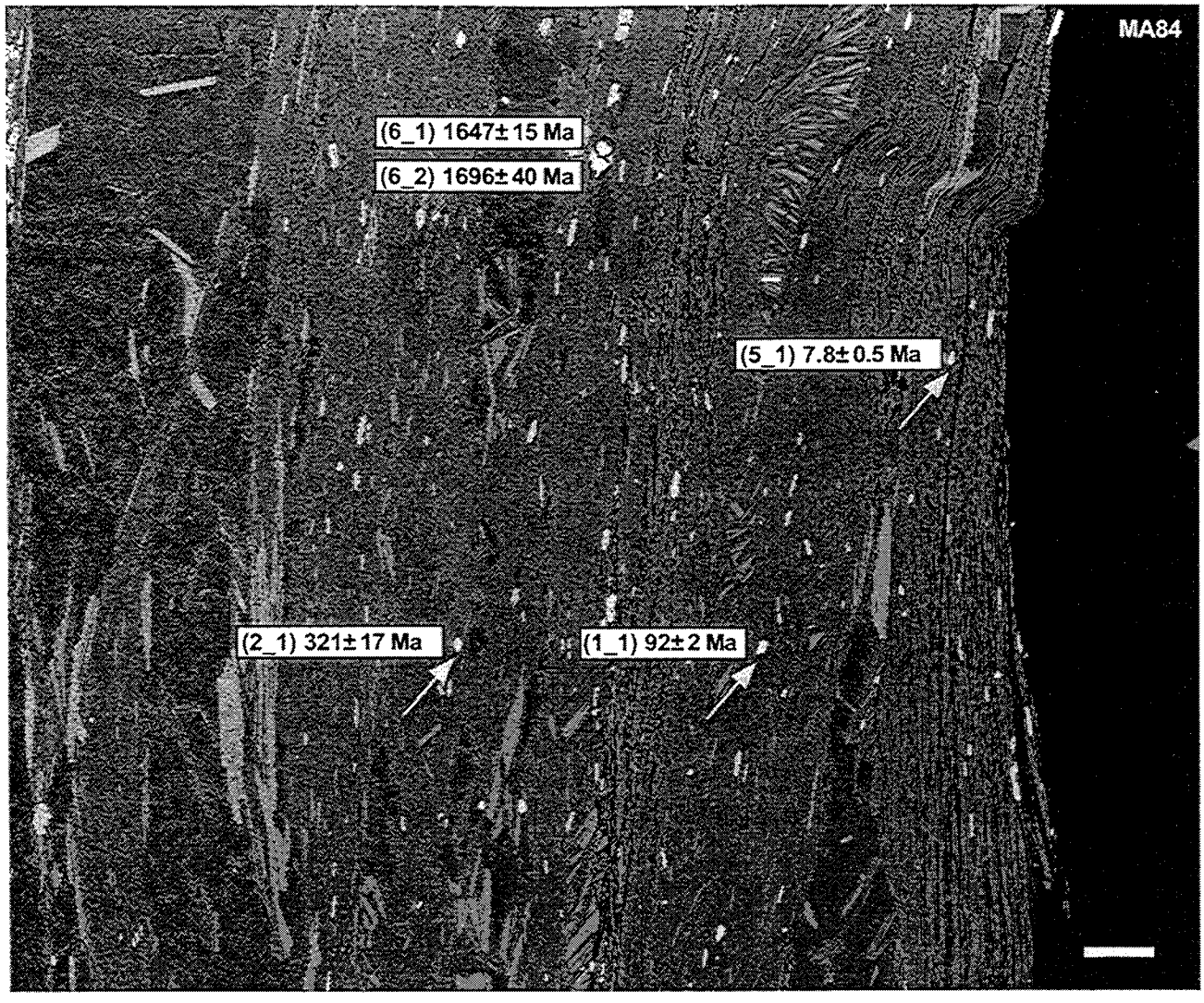

Figure 7. BSE image of domain 3 sample MA84 with age information (1σ) indicated. The scale bar is 100 μm. Details regarding the analyses is available in the data repository.

separation [e.g., *Hodges et al.*, 1992; *Nazarchuk*, 1993; *Hodges et al.*, 1996; *Coleman*, 1998; *Dèzes et al.*, 1999; *Simpson et al.*, 2000]. The striking age difference of grains in sample MA84 (Figure 7) demonstrates the advantage of using an in situ method for rocks that experienced a complicated tectonic history. The ±2% uncertainty in the Th-Pb ion microprobe ages is often superior to results from conventional U-Pb ages typically reported for Himalayan monazites [e.g., *Nazarchuk*, 1993; *Coleman*, 1996b; *Hodges et al.*, 1996; *Coleman*, 1998]. Inaccuracies in the conventional U-Pb method may be due to failure to document an inherited component, variable Pb* loss, instrumental limitations in measuring small amounts of U and Pb, or excess ^{206}Pb [*Schärer*, 1984; *Copeland et al.*, 1988; *Parrish*, 1990; *Coleman*, 1998].

Plate 12 shows the distribution of ion microprobe monazite ages along both transects. To interpret the ages, the P-T history of the rock, textural relationship of the monazite with other phases, uncertainty ion microprobe calibration curve, and fraction of radiogenic ^{208}Pb are evaluated. The significance of the interpreted age, including those obtained from garnet-hosted and matrix grains, can then be judged using models that evaluate potential Pb loss based on temperature, duration, and grain size [e.g., *Smith and Giletti*, 1997]. Uncertainty in grain size is introduced because the thin section only provides a two-dimensional view of the monazite grain

Monazites in hanging wall rocks experienced temperatures above 650°C and yield a range of ages expected due to the strong influence of diffusional Pb loss [*Smith and Giletti*, 1997]. All monazites from domain 3 and those from domain 2 collected more than 5 km south of the MCT (e.g., DH38, MA33) experienced temperatures below 600°C (Figure 4). A 22 Ma monazite grain would have to lose 60% ^{208}Pb to yield an apparent age of 8 Ma. To sustain this amount of loss, a 50-μm monazite grain requires 600°C for >10 m.y. A 200-μm monazite grain held at 600°C for 10 m.y., experiences <15% Pb loss due to diffusion [see *Smith and Giletti*, 1997]. These calculations strongly indicate that dates from monazite grains from domain 3 and lower levels of domain 2 record crystallization ages.

Monazite growth in Himalayan metapelites may be due to

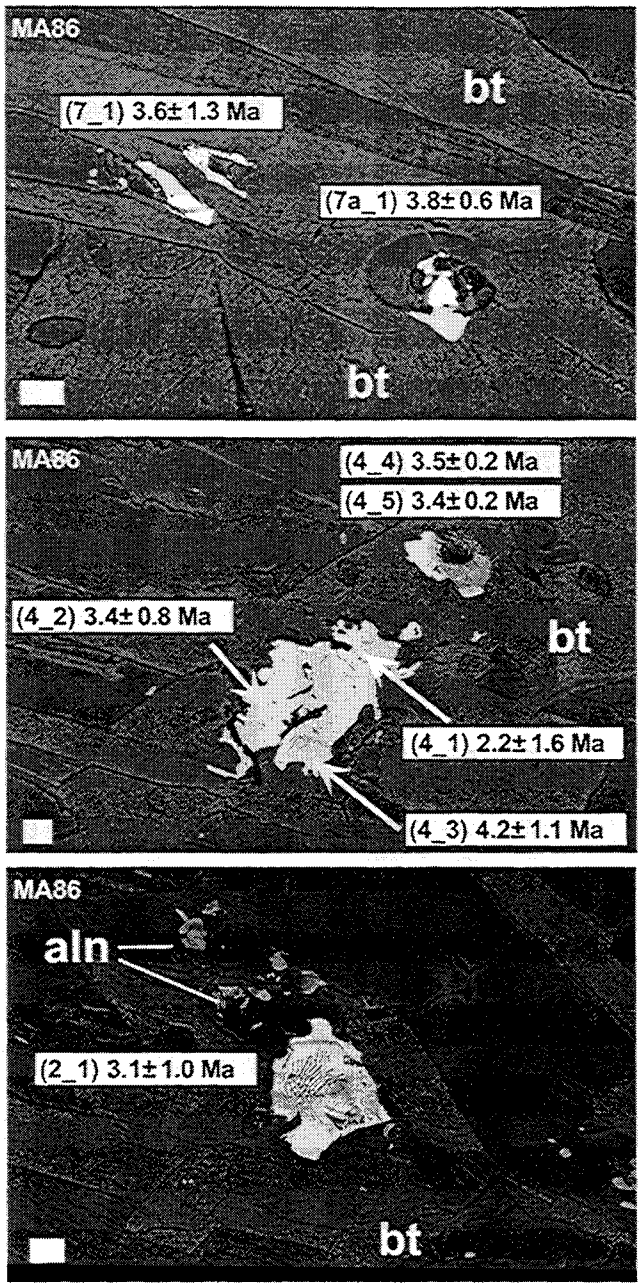

Figure 8. BSE images of domain 3 sample MA86 with age information (1σ) indicated. The scale bar is 10 μm. aln, allanite, bt, biotite. Details regarding the analyses are available in the data repository.

allanite breakdown or dissolution of existing detrital grains. The dissolution-precipitation process is a possible age resetting and Pb loss mechanism [e.g., *Ayers et al.*, 1999]. To ascertain the degree to which this occurred, knowledge of the textural relationship of the monazite grain, distribution of ages within the sample, and the rock's P-T history are required. Some Lesser Himalayan rocks contain evidence of a polyphase history, and dissolution-precipitation is speculated to have a strong influence in these samples (e.g., sample MA84).

Pliocene mica ages have long existed as evidence of late cooling of the MCT shear zone but were attributed to late stage brittle thrusting [*Macfarlane*, 1993] or fluid flow [*Copeland et al.*, 1991]. The youngest monazite grains reported for rocks collected along the Marysandi River MCT transect (3.3±0.1 Ma) require an alternative explanation. The age indicates the area affected by slip within the MCT shear zone extends from the base of the hanging wall gneisses at least to the outcrop that contains sample MA86. Tectonic boundaries within the shear zone are difficult to discern due to poor exposure and the lack of metamorphic or structural discontinuities. Despite detailed field studies, significant changes in lithology, structure, or shear fabrics in rocks that contain evidence of MCT-related activity were not observed [*Colchen et al.*, 1980; *Arita*, 1983]. Sample MA65, collected 2 km west of the main Marysandi River transect, shows a range of monazite ages consistent with a domain 2 sample (Plate 12). These observations suggest that thermobarometric and geochronologic information may be essential in before defining tectonic boundaries within the MCT shear zone.

The MA86 garnet records temperature conditions insufficient to allow significant Pb loss from ~0.1 mm-sized monazite (Figure 4; P ≈ 0.72 GPa; T ≈ 535°C). A hydrothermal origin for the grains seems unlikely because textural evidence of fluid and related alteration are absent. The MA86 garnet preserves prograde compositional zoning, similar to other domain 3 rocks. This sample contains allanite near the monazite grains, suggesting a reaction between the two minerals without influence from a Th- and rare earth element-rich fluid (Figure 8).

9.3. Implications for Evolutionary Models of the Himalaya

If the monazite in MA86 formed at the maximum temperature recorded by the garnet, this rock experienced ~40 km of slip in the last 3 m.y., assuming a 30° MCT ramp. The range of exhumation rates from these calculations is 10-14 mm yr^{-1}. This is ~30% of the total convergence rate between the Indian and Eurasian Plates (44-61 mm yr^{-1} [*Minster and Jordan*, 1978; *Armijo et al.*, 1989; *DeMets et al.*, 1990], and is similar to shortening rates estimated for the MFT (9-16 mm yr^{-1} [*Lyon-Caen and Molnar*, 1985; *Baker et al.*, 1988; *Yeats et al.*, 1992; *Powers et al.*, 1998]). If the average Indo-Himalayan convergence rate is 14±4 mm yr^{-1} [*Powers et al.*, 1998], in central Nepal, 50-70% of this rate appears localized along the MCT shear zone since the Pliocene.

The two classes of models for the origin of inverted metamorphism (one-slip or multislip) can be evaluated using constraints presented in this paper. Models that link MCT slip and hanging wall metamorphism to the creation of the footwall inverted signature are clearly incorrect. Ages of monazite grains immediately beneath domain 1 are consistent with Miocene MCT slip, but the ages decrease with increasing distance south of the fault, indicating late Miocene-Pliocene activity within the shear zone. The age distribution along the drainages (Plate 12) is consistent with a multislip hypothesis (e.g., Figure 2). *Harrison et al.* [1998] developed a thermokinematic model in which the inverted metamorphic sequences underlying the MCT formed by the transposition of right-way-up metamorphic sequences during late Miocene-Pliocene out-of-sequence thrusting. Several aspects are supported by petrologic and thermochronologic constraints.

The MCT juxtaposes the Greater Himalayan Crystallines against the Lesser Himalaya at ~25 Ma. In this scenario, the Greater Himalayan Crystallines has already experienced

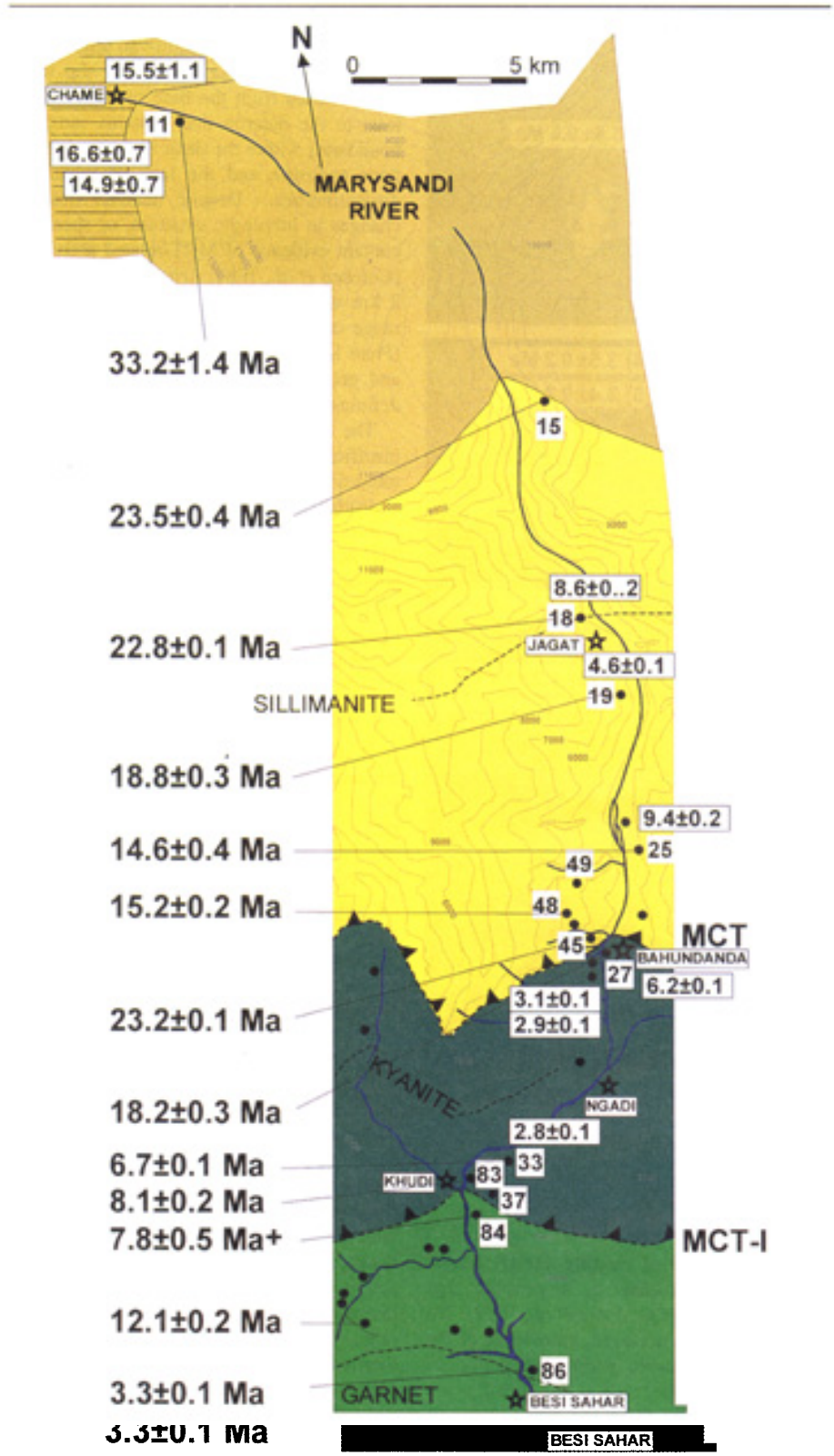

Plate 10. Weighted mean Th-Pb monazite and $^{40}Ar/^{39}Ar$ mica age distribution map along the Marysandi River. The ion microprobe Th-Pb monazite ages are shown in bold numbers, and the $^{40}Ar/^{39}Ar$ mica ages are in boxes. The age of a single monazite grain is noted by a plus. The mica ages are from *Edwards* [1995], *Coleman* [1996b], and *Coleman and Hodges* [1998]. All errors are 1σ.

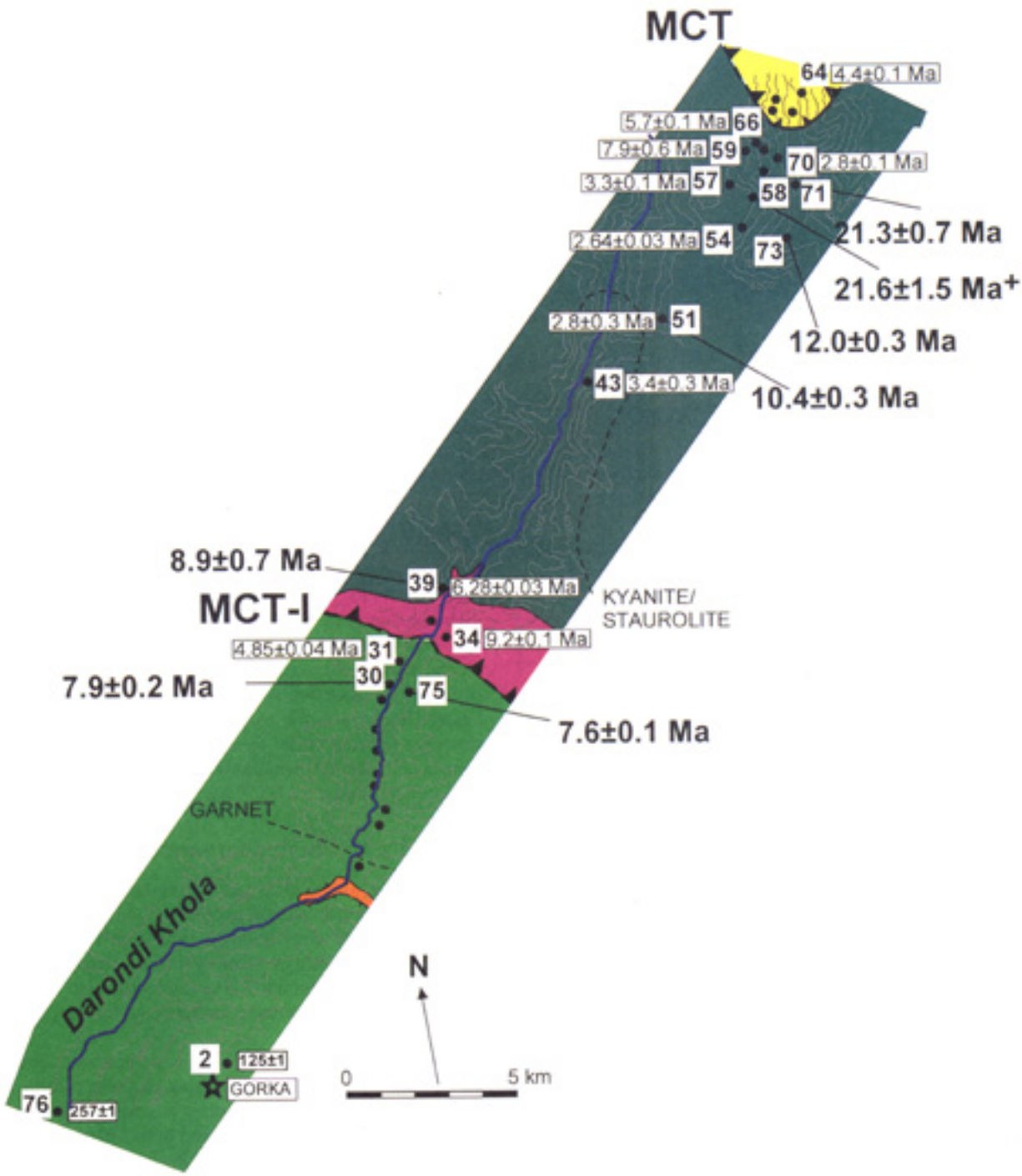

Plate 11. Weighted mean Th-Pb monazite and total gas $^{40}Ar/^{39}Ar$ mica age distribution map along the Darondi Khola. The ion microprobe Th-Pb monazite ages are shown in bold numbers, and the $^{40}Ar/^{39}Ar$ mica ages are in boxes. Ages of single monazite grains are noted by a plus. The mica ages are from this study. All errors are 1σ.

recrystallization due to Eohimalayan metamorphism and thickening. Domain 1 monazite grains should reveal age gradients due to variable diffusive Pb loss and cooling from different depths (Figure 2, right inset). The Harrison et al. [1998] model predicts a hanging wall lithostatic pressure gradient, with the highest pressures and temperatures recorded in rocks collected near the MCT [see *Hubbard*, 1989].

Along the Marysandi transect, monazite grains collected near the MCT record ages from 22 to 18 Ma, whereas monazite ages of from a sample collected near the boundary with the Tethys Formation metasediments yields Eohimalayan ages from 30 to 50 Ma. According to this model, samples collected near the Greater Himalayan Crystallines-Tethys Formation contact are from shallower levels, traveled along

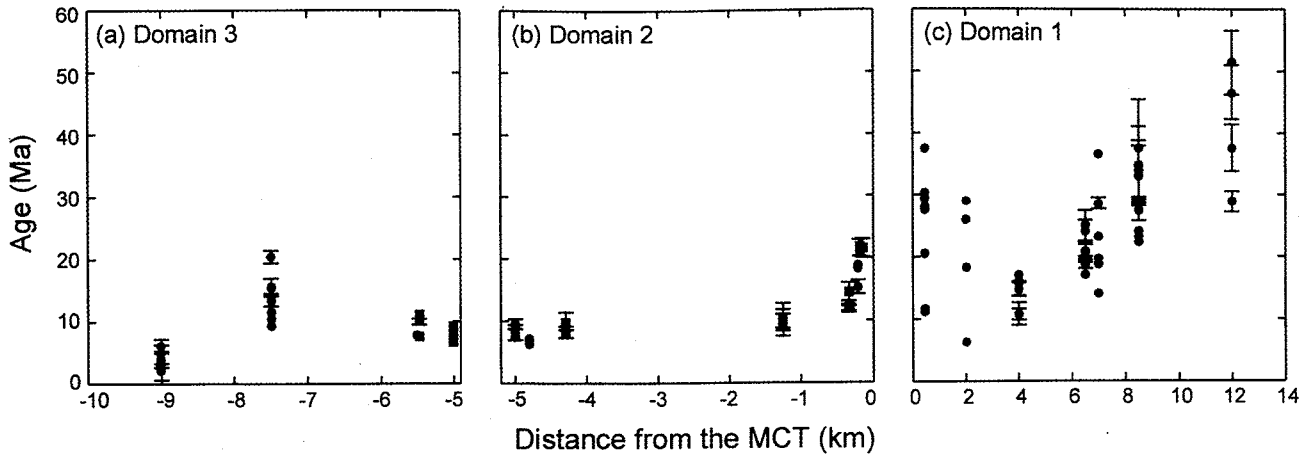

Plate 12. Th-Pb monazite ages from the Darondi Khola and Marysandi River traverse plotted versus structural distance normal to MCT. Each datum represents a single-spot analysis with 1σ error bars. Monazite inclusions in garnet are indicated by red. Only the ages since 60 Ma are plotted in the diagram. Details regarding the analyses are available in the data repository.

the thrust flat, and preserved their Eocene-Oligocene origin, whereas those near the MCT were exhumed from deeper crust along the thrust ramp.

In the *Harrison et al.* [1998] model, the MBT becomes active when slip on the MCT ceases, causing the MCT ramp to climb up the MBT ramp. As a result, the inactive MCT ramp progressively tilts more steeply towards north. During the late Miocene, the locus of thrusting was transferred southward from the MCT to the MCT I. Therefore, the hanging wall rocks of both thrust sheets were moving along the MCT I [e.g., Figure 2, top and left insets]. This scenario is compatible with structural observations that the MCT was warped during development of a Lesser Himalaya duplex system [e.g., *DeCelles et al.*, 1998; *Paudel and Arita*, 2000]. The model predicts that Domain 2 monazite grains should record a polymetamorphic history, whereas Domain 3 samples should contain monazite with late Miocene ages, consistent with activation of the shear zone during that time.

The allanite and monazite ages and garnet zoning pattern from sample MA33, collected at the base of the Domain 2 along the Marysandi River transect are consistent with a polymetamorphic history. P-T paths from samples MA61, DH17, and DH19 suggest the presence of a tectonic and metamorphic break within the MCT footwall. The extensive presence of late Miocene and Pliocene monazite and muscovite ages suggests rapid exhumation of the MCT shear zone at this time.

10. Conclusions

This paper presents thermobarometric data, ion microprobe Th-Pb monazite ages, and muscovite $^{40}Ar/^{39}Ar$ ages from garnet-bearing assemblages collected adjacent to the crustal-scale fault largely responsible for the creation of the highest mountain range on the planet. Th-Pb dating of small (~20-200-μm-sized) monazite grains yield remarkably young ages and reveals evidence of Late Miocene-Pliocene activity of the MCT and development of the underlying shear zone. Pliocene ages of footwall monazite grains imply the MCT shear zone accounts for a significant portion of the convergence rate between India and the Himalaya since ~3 Ma. The inverted metamorphic sequences beneath the MCT ramp appear to form during reactivation of the thrust following ~10 m.y. of inactivity or low slip rates. Thermobarometric results from garnet-bearing assemblages and Th-Pb monazite ages support the idea that the inverted metamorphism characterizing the footwall of the thrust is the result of the accretion of successive tectonic slivers of the Lesser Himalaya to the hanging wall. Results reported here strongly indicate that those models that directly link Himalayan inverted metamorphism with thermal conditions produced by slip on the MCT are incorrect.

Appendix A: Thermobarometric Methods

Data used to calculate the thermobarometric conditions include the original electron microprobe mineral compositions and garnet X-ray element maps (available at http://oro.ess.ucla.edu/argonlab/data_repositiory.html). Details regarding samples from the Darondi Khola transect is also reported by M.J. Kohn et al., submitted manuscript (2000) and *Kohn and Spear* [2001].

Samples chosen for thermobarometric analyses appear in a garnet-bearing assemblage containing biotite ± chlorite as the major Fe-Mg minerals. Chlorite is commonly found near or in contact with the garnets analyzed in this paper. Garnets in close association with chlorite and having textures suggestive of significant retrogression were avoided.

X-ray maps of Mn, Ca, Fe, and Mg were taken of Himalayan garnets using an electron microprobe (Plates 6-8 and Figure 3). A current of 120-200 nA, beam size of ~2 μm, and count times of 30-35 ms gave in the clearest results. The maps were used to qualitatively evaluate garnet zoning patterns and assure areas chosen for quantitative analysis best estimate the pressure and temperature conditions recorded by the assemblage [e.g., *Spear and Peacock*, 1989; *Kohn and Spear*, 2001].

Peak pressures and temperatures recorded by samples adjacent to the MCT were estimated from mineral compositions via thermodynamic calculations. The compositions of garnet, muscovite, plagioclase, biotite, and chlorite were obtained using an electron microprobe operating

at an accelerating potential of 20 kV and a probe current of ~10 nA. Only matrix mineral compositions of biotite, muscovite, and plagioclase were used. Maximum count times were 20 s, and raw data were reduced using the ZAF matrix correction.

Internally consistent thermometer and barometer calibrations were applied using the garnet and matrix mineral compositions. For most samples, garnet-biotite thermometry (*Ferry and Spear* [1978] with the *Berman* [1990] garnet solution model) and garnet-plagioclase-biotite-muscovite barometry [*Hoisch*, 1990] were used to constrain temperature and pressure. The garnet-hornblende geothermometer of *Graham and Powell* [1984] and the barometer of *Kohn and Spear* [1990] were used for sample DH38. Different thermobarometric calibrations change estimated conditions by ±25°C and ±0.1 GPa, but overall trends are unaltered. Only temperatures were estimated for rocks that lack plagioclase (MA83, MA64, MA68, MA58) or muscovite (MA79).

P-T path calculations from garnets displaying prograde zonation were obtained using the methods outlined by *Spear and Selverstone* [1983] and *Spear* [1993]. All rocks were modeled using Progam Gibbs, version 4.7 [*Spear et al.*, 1997], with the observed assemblage garnet + biotite + chlorite + muscovite + plagioclase + quartz in the MnNCKFMASH system. A pure H_2O fluid at lithostatic pressure was also assumed. Activity models unalter trends of retrieved P-T paths [*Kohn*, 1993], and all mineral solutions were assumed ideal, except garnet for which the *Berman* [1990] model was used. Staurolite, chloritoid, or carbonate minerals are absent in these samples. Chemical zoning in the garnets analyzed is smooth and consistent with growth in the observed assemblage. Plagioclase grains have higher-Ca cores and lower-Ca rims, the expected consequence of garnet growth and fractional crystallization as the mineral depletes the remaining matrix in Ca [*Spear et al.*, 1990]. Most paths are two-point core-rim paths, except for some Darondi Khola samples for which an intermediate point was used.

Appendix B: Th-Pb Ion Microprobe Dating Methods

Details of the ion microprobe analyses include BSE images of each monazite grain dated and isotopic data (available at http://oro.ess.ucla.edu/argonlab/data_repositiory.html).

Monazite grains were located in thin sections using backscattered electron (BSE) petrography and energy dispersive X-ray spectroscopy with a scanning electron microscope or electron microprobe. Many are zoned, irregularly shaped, and vary in size from 20 to 200 μm. Monazite grains suitable for ion microprobe analysis were documented with detailed BSE images. The portion of the thin section containing the grains of interest was then removed using a precision saw and mounted in epoxy with approximately five grains of polished age standards (monazite 554 [see *Harrison et al.*, 1999b]). To aid in grain relocation using the ion microprobe, reflected light images were taken of the 1-inch ion microprobe mount using an optical microscope fitted with a digital camera. The sample was cleaned in distilled water and high-purity ultrasonic cleanser, and carbon or gold coated.

Monazite grains were analyzed using a CAMECA ims 1270 ion microprobe. The dating method takes advantage of the kinetic energy distribution of the Th and Pb ions sputtered from monazite using a primary oxygen (O^-) beam focused to a spot size that varied from ~5 to 30 μm in size (*see Harrison et al.* [1995, 1999b] for details). The primary beam varied from 2 to 20 nA. Typically, a 50 eV energy window and a ~10 eV offset for Th^+ were used. At a mass resolving power of ~6000, all Pb and Th isotopes were resolved from any significant molecular interferences. The O^- beam sputtered less than a micron of the grain surfaces, and results were available within a few minutes. The uncertainty in the Th-Pb monazite ages reported in this paper is limited by the reproduction of a calibration curve and is ±1-2%.

Appendix C: $^{40}Ar/^{39}Ar$ Muscovite Dating Methods

Details of the muscovite analyses include isotopic data and inverse isochron plots (available at http://oro.ess.ucla.edu/argonlab/data_repositiory.html).

High-purity concentrates of muscovite grains were separated from 20 rocks collected along the Darondi Khola MCT transect and analyzed using the $^{40}Ar/^{39}Ar$ method with a VG 3600 automated mass spectrometer. The samples were irradiated in the Ford Reactor at the University of Michigan. The J factor, determined from Fish Canyon sanidine (27.8 Ma) flux monitors, is ~0.007 for all samples. About 10 mg of muscovite from each rock was step heated within a double vacuum furnace.

Acknowledgments. This project was supported by funding from the Institute of Geophysics and Planetary Physics-Lawrence Livermore National Laboratory University Collaborative Research Program 97-GS002 and the National Science Foundation. We acknowledge facility support from the Instrumentation and Facilities Program of the National Science Foundation. We thank An Yin, Frank Spear, Mary Hubbard, and Roberta Rudnick for providing valuable and constructive reviews of the manuscript and Chris Coath for assistance with in situ monazite ion-microprobe analysis.

References

Arita, K., Origin of the inverted metamorphism of the Lower Himalaya, central Nepal, *Tectonophysics*, *95*, 43-60, 1983.

Armijo, R., P. Tapponnier, J.L. Mercier, and H. Tonglin, Quaternary extension in southern Tibet: Field observations and tectonic implications, *J. Geophys. Res.*, *91*, 13,803-13,872, 1986.

Ayers, J.C., C. Miller, B. Gorisch, and J. Milleman, Textural development of monazite during high-grade metamorphism: Hydrothermal growth kinetics, with implications for U, Th-Pb geochronology, *Am. Mineral.*, *84*, 1766-1780, 1999.

Baker, D.M., R.J. Lillie, R.S. Yeats, G.D. Johnson, M. Yousuf, and A.S.H. Zamin, Development of the Himalayan frontal thrust zone: Salt Range, Pakistan, *Geology*, *16*, 3-7, 1988.

Balasubramaniyam, M.N., M.K. Murthy, D.K. Paul, and A.K. Sarkar, K-Ar ages of Indian kimberlites, *J. Geol. Soc. India*, *19*, 548-585, 1978.

Berman, R.G., Mixing properties of Ca-Mg-Fe-Mn garnets, *Am. Mineral.*, *75*, 328-344, 1990.

Bordet, P., M. Colchen, and P. Le Fort, Recherches géologiques dans l'Himalaya du Népal, région du Nyi-Shang, 138 pp., Cent. Nat. de la Rech. Sci., Paris, 1975.

Brown, R.L., and J.H. Nazarchuk, Annapurna detachment fault in the Greater Himalaya of central Nepal, in *Himalayan Tectonics*, edited by P.J. Trealor and M.P. Searle, *Spec. Publ. Geol. Soc. London*, *74*, 461-473, 1993.

Brunel, M., and J.R. Kienast, Etude pétro-structurale des chevauchements ductiles Himalayens sur la transversale de l'Everest-Makalu (Nepal oriental), *Can. J. Earth Sci.*, *23*, 1117-1137, 1986.

Burchfiel, C.B., Chen Zhiliang, K.V. Hodges, Liu Yuping, L.H. Royden, Deng Changrong, and Xu Jiene, The Southern Tibetan Detachment System, Himalayan orogen: Extension contemporaneous with and parallel to shortening in a collisional mountain belt, *Spec. Pap. Geol. Soc. Am., 269*, 1-40, 1992.

Burg, J.P., M. Brunel, D. Gapais, G.M. Chen, and G.H. Liu, Deformation of leucogranites of the crystalline Main Central Sheet in southern Tibet (China), *J. Struct. Geol., 6*, 535-542, 1984.

Catlos, E.J., S.S. Sorensen, and T.M. Harrison, Th-Pb ion microprobe dating of allanite, *Am. Mineral., 85*, 633-648, 2000.

Chakraborty, S., and J. Ganguly, Compositional zoning and cation diffusion in garnets, in *Diffusion, Atomic Ordering and Mass Transport*, edited by J. Ganguly, Springer-Verlag, New York, pp.120-175, 1991.

Chen, Z., B.C. Burchfiel, Y. Liu, R.W. King, L.H. Royden, W. Tang, E. Wang, J. Zhao, and X. Zhang, Global Positioning System measurements from eastern Tibet and their implications for India/Eurasia intercontinental deformation, *J. Geophys. Res., 105*, 16,215-16,277, 2000.

Colchen, M., P. Le Fort, and A. Pêcher, Annapurna-Manaslu-Ganesh Himal, 136 pp., Cent. Nat. de la Rech. Sci., Paris, 1980.

Coleman, M.E., Orogen-parallel and orogen-perpendicular extension in the central Nepalese Himalayas, *Geol. Soc. Am. Bull., 108*, 1594-1607, 1996a.

Coleman, M.E., The tectonic evolution of the central Himalaya, Marsyandi Valley, Nepal, Ph.D. dissertation, Mass. Inst. of Technol., Cambridge, 1996b.

Coleman, M.E., U-Pb constraints on Oligocene-Miocene deformation and anatexis within the central Himalaya, Marsyandi Valley, Nepal, *Am. J. Sci., 298*, 553-571, 1998.

Coleman, M.E., and K.V. Hodges, Contrasting Oligocene and Miocene thermal histories from the hanging wall and footwall of the South Tibetan detachment in the central Nepal Himalaya from $^{40}Ar/^{39}Ar$ thermochronology, Marsyandi Valley, central Nepal, *Tectonics, 17*, 726-740, 1998.

Copeland, P., R.R. Parrish, and T.M. Harrison, Identification of inherited radiogenic Pb in monazite and its implications for U-Pb systematics, *Nature, 333*, 760-763, 1988.

Copeland, P., T.M. Harrison, K.V. Hodges, P. Maruéjol, P. Le Fort, and A. Pêcher, An early Pliocene thermal disturbance of the Main Central Thrust, central Nepal: Implications for Himalayan tectonics, *J. Geophys. Res., 96*, 8475-8500, 1991.

Davidson, C., D.E. Grujic, L.S. Hollister, and S.M. Schmid, Metamorphic reactions related to decompression and synkinematic intrusion of leucogranite, High Himalayan Crystallines, Bhutan, *J. Metamorph. Geol., 15*, 593-612, 1997.

DeCelles, P.G., G.E. Gehrels, J. Quade, T.P. Ojha, P.A. Kapp, and B.N. Upreti, Neogene foreland basin deposits, erosional unroofing, and the kinematic history of the Himalayan fold-thrust belt, western Nepal, *Geol. Soc. Am. Bull., 110*, 2-21, 1998.

DeMets, C., R.G. Gordon, D.F. Argus, and S. Stein, Current plate motions, *Geophys. J. Int., 101*, 425-478, 1990.

Dèzes, P.J., J.-C. Vannay, A. Steck, F. Bussy, and M. Cosca, Synorogenic extension: Quantitative constraints on the age and displacement of the Zanskar Shear Zone (northwest Himalaya), *Geol. Soc. Am. Bull., 111*, 364-374, 1999.

Edwards, R.M., $^{40}Ar/^{39}$ Ar geochronology of the Main Central Thrust (MCT) region; evidence for late Miocene to Pliocene disturbances along the MCT, Marsyangdi River valley, west-central Nepal Himalaya, *J. Nepal Geol. Soc., 10*, 41-46, 1995.

Edwards, M.A., and T.M. Harrison, When did the roof collapse? Late Miocene north-south extension in the high Himalaya revealed by Th-Pb monazite dating of the Khula Kangri granite, *Geology, 25*, 543-546, 1997.

England, P., and P. Molnar, The interpretation of inverted metamorphic isograds using simple physical calculations, *Tectonics, 12*, 145-157, 1993.

England, P., P. Le Fort, P. Molnar, and A. Pêcher, Heat sources for Tertiary metamorphism and anatexis in the Annapurna-Manaslu region, central Nepal, *J. Geophys. Res., 97*, 2107-2128, 1992.

Ferry, J.M., and F.S. Spear, Experimental calibration of partitioning of Fe and Mg between biotite and garnet, *Contrib. Mineral. Petrol., 66*, 113-117, 1978.

Florence, F.P., and F.S. Spear, Effects of diffusional modification of garnet growth zoning on P-T path calculations, *Contrib. Mineral. Petrol., 107*, 487-500, 1991.

Fuchs, G., R.W. Widder, and R. Tuladhar, Contributions to the geology of the Annapurna Range (Manang Area, Nepal), *Geol. Jahrb. Reihe B-A, 131*, 593-607, 1988.

Fuchs, G., K. Regmi, and E. Schill, Note on the geology of the Nar-Manang Region in northern Nepal (Himalaya), 14th Himalaya-Karakoram-Tibet Workshop, Kloster Ettal, Germany, *Terra Nostra, 99*(2), 46-47, 1999.

Gansser, A., The geodynamic history of the Himalaya, in *Zagros, Hindu Kush, Himalayan Geodynamic Evolution, Geodyn. Ser.*, vol.3, edited by H.K. Gupta and F.M. Delany, pp.111-121, AGU, Washington, D. C., 1981.

Graham, C.M., and R. Powell, A garnet-hornblende geothermometer: Calibration, testing, and application to the Pelona Schist, southern California, *J. Metamorph. Geol., 2*, 13-31, 1984.

Grove, M., and T.M. Harrison, Monazite Th-Pb age depth profiling, *Geology, 27*, 487-490, 1999.

Guillot, S., An overview of the metamorphic evolution in central Nepal, *J. Asian Earth Sci., 17*, 713-725, 1999.

Guillot, S., A. Pêcher, P. Rochette, and P. Le Fort, The emplacement of the Manaslu granite of central Nepal: Field and magnetic susceptibility constraints, in *Himalayan Tectonics*, edited by P.J. Trealor and M.P. Searle, *Spec. Publ. Geol. Soc. London, 74*, 413-428, 1993.

Harris, N., and J. Massey, Decompression and anatexis of Himalayan metapelites, *Tectonics, 13*, 1537-1546, 1994.

Harris, N., S. Inger, and J. Massey, The role of fluids in the formation of High Himalayan leucogranites, in *Himalayan Tectonics*, edited by P.J. Trealor and M.P. Searle, *Spec. Publ. Geol. Soc. London, 74*, 391-400, 1993.

Harrison, T.M., K.D. McKeegan, and P. Le Fort, Detection of inherited monazite in the Manaslu leucogranite by $^{208}Pb/^{232}Th$ ion microprobe dating: Crystallization age and tectonic implications, *Earth Planet. Sci. Lett., 133*, 271-282, 1995.

Harrison, T.M., M. Grove, and O.M. Lovera, New insights into the origin of two contrasting Himalayan granite belts, *Geology, 25*, 899-902, 1997.

Harrison, T.M., M. Grove, O.M. Lovera, and E.J. Catlos, A model for the origin on Himalayan anatexis and inverted metamorphism, *J. Geophys. Res., 103*, 27,017-27,032, 1998.

Harrison, T.M., M. Grove, O.M. Lovera, E.J. Catlos, and J. D'Andrea, The origin of Himalayan anatexis and inverted metamorphism: Models and constraints, *J. Asian Earth Sci., 17*, 755-772, 1999a.

Harrison, T.M., M. Grove, K.D. McKeegan, C.D. Coath, O.M. Lovera, and P. Le Fort, Origin and emplacement of the Manaslu intrusive complex, central Himalaya, *J. Petrol., 40*, 3-19, 1999b.

Hinton, R.W., Ion microprobe analysis in geology, in *Microprobe Techniques in the Earth Sciences*, edited by P.J. Potts et al., Chapman and Hall, New York, pp. 235-289, 1995.

Hodges, K.V., and D.S. Silverberg, Thermal evolution of the Greater Himalaya, Garhwal, India, *Tectonics, 7*, 583-600, 1988.

Hodges, K.V., P. Le Fort, and A. Pêcher, Possible thermal buffering by crustal anatexis in collisional orogens: Thermobarometric evidence from the Nepalese Himalaya, *Geology, 16*, 707-710, 1988.

Hodges, K.V., R.R. Parrish, T.B. Housh, D.R. Lux, B.C. Burchfiel, L.H. Royden, and Z. Chen, Simultaneous Miocene extension and shortening in the Himalayan orogen, *Science, 258*, 1466-1470, 1992.

Hodges, K.V., B.C. Burchfiel, L.H. Royden, Z. Chen, and Y. Liu, The metamorphic signature of contemporaneous extension and shortening in the central Himalayan orogen: Data from the Nyalam transect, southern Tibet, *J. Metamorph. Geol., 11*, 721-737, 1993.

Hodges, K.V., R.R. Parrish, and M.P. Searle, Tectonic evolution of the central Annapurna Range, Nepalese Himalayas, *Tectonics, 15*, 1264-1291, 1996.

Hoisch, T.D., Empirical calibration of six geobarometers for the mineral assemblage quartz + muscovite + biotite + plagioclase + garnet, *Contrib. Mineral. Petrol., 104*, 225-234, 1990.

Hubbard, M.S., Thermobarometric constraints on the thermal history of the Main Central Thrust Zone and Tibet Slab, eastern Nepal Himalaya, *J. Metamorph. Geol., 7*, 19-30, 1989.

Hubbard, M.S., Ductile shear as a cause of inverted metamorphism: Example from the Nepal Himalaya, *J. Geol.*, *104*, 493-499, 1996.

Huerta, A.D., L.H. Royden, and K.V. Hodges, The interdependence of deformational and thermal processes in mountain belts, *Science*, *273*, 637-639, 1996.

Inger, S., and N.B.W. Harris, Tectonothermal evolution of the High Himalaya Crystalline sequence, Langtang Valley, northern Nepal, *J. Metamorph. Geol.*, *10*, 439-452, 1992.

Jäger, E., Introduction to geochronology, in *Lectures in Isotope Geology*, edited by E. Jäger and J.C. Hunziker, pp.1-12, Springer-Verlag, New York, 1979.

Kaneko, Y., Thermal structure in the Annapurna region, central Nepal Himalaya: Implication for the inverted metamorphism, *J. Mineral. Petrol. Econ. Geol.*, *90*, 143-154, 1995.

Kayal, J.R., Precursor seismicity, foreshocks and aftershocks of the Uttarkashi earthquake of October 20, 1991 at Garhwal Himalaya, *Tectonophysics*, *263*, 339-345, 1996.

Khattri, K.N., and A.K. Tyagi, Seismicity patterns in the Himalayan plate boundary and identification of areas of high seismic potential, *Tectonophysics*, *96*, 281-297, 1983.

Kingsbury, J.A., C.F. Miller, J.L. Wooden, and T.M. Harrison, Monazite paragenesis and U-Pb systematics in rocks of the eastern Mojave Desert, California, U.S.A.: Implications for thermochronometry, *Chem. Geol.*, *110*, 147-167, 1993.

Kohn, M.J., Uncertainties in differential thermodynamic (Gibbs Method) P-T paths, *Contrib. Mineral. Petrol.*, *113*, 24-39, 1993.

Kohn, M.J., and F.S. Spear, Two new barometers for garnet amphibolites with applications to eastern Vermont, *Am. Mineral.*, *75*, 89-96, 1990.

Kohn, M.J., and F.S. Spear, Retrograde net transfer reaction (ReNTR) insurance for P-T estimates, *Geology*, *28*, 1127-1130, 2001.

Kohn, M.J., E.J. Catlos, F.J. Ryerson, and T.M. Harrison, Metamorphic P-T discontinuity at the base of the MCT zone, central Nepal, *Eos Trans. AGU, 80*(46) Fall Meet. Suppl., F990, 1999.

Lavé, J., and J.P. Avouac, Active folding of fluvial terraces across the Siwaliks Hills, Himalayas of central Nepal, *J. Geophys. Res.*, *105*, 5735-5770, 2000.

Le Fort, P., Himalayas, the collided range: Present knowledge of the continental arc, *Am. J. Sci.*, *275A*, 1-44, 1975.

Le Fort, P., Evolution of the Himalaya, in *The Tectonic Evolution of Asia*, edited by A. Yin and T.M. Harrison, pp. 95-109, Cambridge Univ. Press, New York, 1996.

Le Fort, P., and S. Guillot, Preliminary results of Himlung expedition to northern Manaslu massif, central Nepal, *Geol. Bull. Spec. Issue*, *31*, 110-112, 1998.

Le Fort, P., F. Debon, A. Pêcher, and A.V.P. Sonet, The 500 Ma magmatic event in alpine southern Asia, a thermal episode at Gondwana scale, in *Évolution des Domains Orogéniques d'Asie Méridionale (de la Turquie à l'Indoneasie)*, edited by P. Le Fort, M. Colchen, and C. Montenat, *Sci. Terre, 47*, 191-209, 1986.

Lyon-Caen, H., and P. Molnar, Constraints on the structure of the Himalaya from the analysis of gravity anomalies and a flexural model of the lithosphere, *J. Geophys. Res.*, *88*, 8171-8191, 1983.

Macfarlane, A.M., The chronology of tectonic events in the crystalline core of the Himalaya, Langtang National Park, central Nepal, *Tectonics*, *12*, 1004-1025, 1993.

Macfarlane, A.M., An evaluation of the inverted metamorphic gradient at Langtang National Park, central Nepal Himalaya, *J. Metamorph. Geol.*, *13*, 595-612, 1995.

Macfarlane, A.M., The metamorphic history of the crystalline rocks in the high Himalaya, Nepal: Insights from thermobarometric data, *J. Asian Earth Sci.*, *17*, 741-753, 1999.

Meigs, A.J., D.W. Burbank, and R.A. Beck, Middle-late Miocene (>10 Ma) formation of the Main Boundary Thrust in the western Himalaya, *Geology*, *23*, 423-426, 1995.

Meldrum, A., L.A. Boatner, W.J. Weber, and R.C. Ewing, Radiation damage in zircon and monazite, *Geochim. Cosmochim. Acta*, *62*, 2509-2520, 1998.

Metcalfe, R.P., Pressure, temperature and time constraints on metamorphism across the Main Central Thrust zone and High Himalaya Slab in the Garhwal Himalaya, in *Himalayan Tectonics*, edited by P.J. Trealor and M.P. Searle, *Spec. Publ. Geol. Soc. London*, *74*, 485-509, 1993.

Minster, J.B., and T.H. Jordan, Present-day plate motions, *J. Geophys. Res.*, *83*, 5331-5354, 1978.

Montel, J., Some good reasons for monazite to be concordant, *J. Conf. Abstr. EUG, 10*, 800, 1999.

Montel, J., J. Kornprobst, and D. Vielzeuf, Preservation of old U-Th-Pb ages in shielded monazite: Example from Beni Bousera Hercynian kinzigites (Morocco), *J. Metamorph. Geol.*, *18*, 335-342, 2000.

Nazarchuk, J.H., Structure and geochronology of the Greater Himalaya, Kali Gandaki region, west-central Nepal, Masters thesis, 157 pp., Carleton Univ., Ottawa, Ont., 1993.

Nelson, K.D., et al., Partially molten crust beneath southern Tibet: Synthesis of project INDEPTH results, *Science*, *274*, 1684-1688, 1996.

Ni, J., and M. Barazangi, Seismotectonics of the Himalayan collision zone; geometry of the underthrusting Indian Plate beneath the Himalaya, *J. Geophys. Res.*, *89*, 1147-1163, 1984.

Overstreet, W.C., The geologic occurrence of monazite, *U.S. Geol. Surv. Prof. Pap.*, *530*, 1-327, 1967.

Parrish, R.R., U-Pb dating of monazite and its application to geological problems, *Can. J. Earth Sci.*, *27*, 1431-1450, 1990.

Parrish, R.R., and K.V. Hodges, Isotopic constraints on the age and provenance of the Lesser and Greater Himalayan sequences, Nepalese Himalaya, *Geol. Soc. Am. Bull.*, *108*, 909-911, 1996.

Paudel, L.P., and K. Arita, Tectonic and polymetamorphic history of the Lesser Himalaya in central Nepal, *J. Asian Earth Sci., 18*, 561-584, 2000.

Pêcher, A., The metamorphism in the central Himalaya, *J. Metamorph. Geol.*, *7*, 31-41, 1989.

Pêcher, A., and P. Le Fort, The metamorphism in central Himalaya, its relations with the thrust tectonic, in *Évolution des Domains Orogéniques d'Asie Méridionale (de la Turquie à l'Indoneasie)*, edited by P. Le Fort, M. Colchen, and C. Montenat, *Sci. Terre, 47*, 285-309, 1986.

Pognante, U., and P. Benna, Metamorphic zonation, migmitization and leucogranites along the Everest transect of eastern Nepal and Tibet: Record of an exhumation history, in *Himalayan Tectonics*, edited by P.J. Trealor and M.P. Searle, *Spec. Publ. Geol. Soc. London*, *74*, 323-340, 1993.

Powers, P.M., R.J. Lillie, and R.S. Yeats, Structure and shortening of the Kangra and Dehra Dun reentrants, sub-Himalaya, India, *Geol. Soc. Am. Bull.*, *110*, 1010-1027, 1998.

Purdy, J.W., and E. Jäger, K-Ar ages on rock-forming minerals from the Central Alps, *Mem. Istit. Geol. Mineral. Univ. Padova*, *30*, 31pp., 1976.

Quidelleur, X., M. Grove, O.M. Lovera, T.M. Harrison, and A. Yin, Thermal evolution and slip history of the Renbu Zedong Thrust, southeastern Tibet, *J. Geophys. Res*, *102*, 2659-2679, 1997.

Rowley, D.B., Age of collision between India and Asia: A review of the stratigraphic data, *Earth Planet. Sci. Lett.*, *145*, 1-13, 1996.

Schärer, U., The effect of initial ^{230}Th disequilibrium on young U-Pb ages: The Makalu case, Himalaya, *Earth Planet. Sci. Lett.*, *67*, 191-204, 1984.

Schelling, D., The tectonostratigraphy and structure of the eastern Nepal Himalaya, *Tectonics*, *11*, 925-943, 1992.

Schelling, D., and K. Arita, Thrust tectonics, crustal shortening, and the structure of the far-eastern Nepal Himalayas, *Tectonics*, *10*, 851-862, 1991.

Schneider, C., and L. Masch, The metamorphism of the Tibet Series from the Manang area, Marsyandi Valley, central Nepal, in *Himalayan Tectonics*, edited by P.J. Trealor and M.P. Searle, *Spec. Publ. Geol. Soc. London*, *74*, 357-374, 1993.

Searle, M.P., and D.C. Rex, Thermal model for the Zanskar Himalaya, *J. Metamorph. Geol.*, *7*, 127-134, 1989.

Seeber, L., and V. Gornitz, River profiles along the Himalayan arc as indicators of active tectonics, *Tectonophysics*, *92*, 335-367, 1983.

Seeber, L., J.G. Armbruster, and R. Quittmeyer, Seismicity and continental subduction in the Himalayan arc, in *Zagros, Hindu Kush, Himalayan Geodynamic Evolution, Geodyn. Ser.*, vol.3, edited by H.K. Gupta and F.M. Delany, pp. 215-242, AGU, Washington, D. C., 1981.

Shen, Zheng-kang, Chengkun Zhao, An Yin, Yanxing Li, D.D. Jackson, Peng Fang, and Danan Dong, Contemporary crustal deformation in east Asia constrained by Global Positioning System measurements, *J. Geophys. Res., 105*, 5721-5734, 2000.

Simpson, R.L., R.R. Parrish, M.P. Searle, and D.J. Waters, Two episodes of monazite crystallization during metamorphism and crustal melting in the Everest region of the Nepalese Himalaya, *Geology*, *28*, 403-406, 2000.

Smith, H.A., and B. Barreiro, Monazite U-Pb dating of staurolite grade metamorphism in pelitic schists, *Contrib. Mineral. Petrol.*, *105*, 602-615, 1990.

Smith, H.A., and B.J. Giletti, Lead diffusion in monazite, *Geochim. Cosmochim. Acta*, *61*, 1047-1055, 1997.

Spear, F.S., *Metamorphic Phase Equilibria and Pressure-Temperature-Time Paths*, 799pp., Mineral. Soc. of Am., Washington, D. C., 1993.

Spear, F.S., and R.R. Parrish, Petrology and cooling rates of the Valhalla Complex, British Columbia, Canada, *J. Petrol.*, *37*, 733-765, 1996.

Spear, F.S., and S.M. Peacock, *Metamorphic Pressure-Temperature-Time Paths*, *Short Course Geol.*, vol.7, 102pp., AGU, Washington D. C., 1989.

Spear, F.S., and J. Selverstone, Quantitative P-T paths from zoned minerals: Theory and tectonic applications, *Contrib. Mineral. Petrol.*, *83*, 348-357, 1983.

Spear, F.S., J. Selverstone, D. Hickmott, P. Crowley, and K.V. Hodges, P-T paths from garnet zoning: A new technique for deciphering tectonic processes in crystalline terranes, *Geology*, *12*, 87-90, 1984.

Spear, F.S., M.J. Kohn, F.P. Florence, and T. Menard, A model for garnet and plagioclase growth in pelitic schists: Implications for thermobarometry and P-T path determinations, *J. Metamorph. Geol.*, *8*, 683-696, 1990.

Spear, F.S., M.J. Kohn, T. Menard, and F. Florence, Program Gibbs, version 4.7, 132pp., *Rensselaer Polytech. Inst.*, Troy, N. Y., 1997.

Srivastava, P., and G. Mitra, Thrust geometries and deep structure of the outer and lesser Himalaya Kumaon and Garhwal (India): Implications for evolution of the Himalayan fold-and-thrust belt, *Tectonics*, *13*, 89-109, 1994.

Stacey, J.S., and J.D. Kramers, Approximate of terrestrial lead isotope evolution by a two-stage model, *Earth Planet. Sci. Lett.*, *26*, 207-221, 1975.

Tracy, R.J., P. Robinson, and A.B. Thompson, Garnet composition and zoning in the determination of temperature and pressure if metamorphism, central Massachusetts, *Am. Mineral.*, *61*, 762-775, 1976.

Upreti, B.N., An overview of the stratigraphy and tectonics of the Nepal Himalaya, *J. Asian Earth Sci.*, *17*, 741-753, 1999.

Valdiya, K.S., Tectonics and the evolution of the central sector of the Himalaya, *Philos. Trans. R. Soc. London, Ser.A*, *326*, 151-175, 1988.

Valdiya, K.S., The Main Boundary Thrust Zone of the Himalaya, India, *Annal. Tectonicae*, *6*, suppl., 54-84, 1992.

Valdiya, K.S., Strong-motion earthquakes in Himalaya-Geological Perspective, *Current Sci. India*, *67*, 313-323, 1994.

Vannay, J.-C., and B. Grasemann, Inverted metamorphism in the High Himalaya of Himachal Pradesh (NW India): Phase equilibria versus thermobarometry, *Schweiz. Mineral. Petrogr. Mitt.*, *78*, 107-132, 1998.

Vannay, J-C., and K.V. Hodges, Tectonometamorphic evolution of the Himalayan metamorphic core between Annapurna and Dhaulagiri, central Nepal, *J. Metamorph. Geol.*, *14*, 635-656, 1996.

Wing, B.A., J.M. Ferry, and T.M. Harrison, The age of andalusite and kyanite isograds in New England from Th-Pb ion microprobe dating of monazite, *Geol. Soc. Am., Abstr. Programs, 31*, A-40, 1999.

Ye, Hong, Wen-yu Zhang, Yu Zhi-shui, and Xia Qin, The seismicity and regional crustal movement in the Himalaya region, in *Geological and Ecological studies of the Qinghai-Xizang Plateau: Proceedings of Symposium on Qinghai-Xizang (Tibet) Plateau (Beijing, China)*, vol.1, pp.65-70, Gordon and Breach, New York, 1981.

Yeats, R.S., T. Nakata, A. Farah, M. Fort, M.A. Mirza, M.R. Pandey, and R.S. Stein, The Himalayan Frontal Fault System, *Annal. Tectonicae*, *6*, suppl., 85-98, 1992.

Yin, A., T.M. Harrison, F.J. Ryerson, C. Wenji, W.S.F. Kidd, and P. Copeland, Tertiary structural evolution of the Gangdese Thrust system, southeastern Tibet, *J. Geophys. Res.*, *99*, 18,175-18,201, 1994.

Zhao, W., K.D. Nelson, and Project INDEPTH, Deep seismic reflection evidence for continental underthrusting beneath southern Tibet, *Nature*, *366*, 557-559, 1993.

E. J. Catlos, M. Grove, T. M. Harrison, and C. E. Manning, Department of Earth and Space Sciences, 3806 Geology, University of California, Los Angeles, CA 90095-1667. (catlos@argon.ess.ucla.edu; marty@oro.ess.ucla.edu; tmh@argon.ess.ucla.edu; manning@ess.ucla.edu)

M. J. Kohn, Department of Geological Sciences, University of South Carolina, Columbia, SC 29208. (mjk@geol.sc.edu)

F. J. Ryerson, Lawrence Livermore National Laboratory, L 202, P.O. Box 808, Livermore, CA 94602. (ryerson1@llnl.gov)

B. N. Upreti, Department of Geology, Tri-Chandra Campus, Tribhuvan University, Kathmandu, Nepal. (bnupreti@wlink.com.np)

(Received April 20, 2000; revised September 22, 2000; accepted October 10, 2000.)